

A Correlation between Flight-determined Lateral Derivatives and Ground-based Data for the Pilatus PC 9/A Training Aircraft in Cruise Configuration

Hilary A. Keating, Nick van Bronswijk, Andrew D. Snowden and Jan S. Drobik

DSTO-TR-0988

DTC QUALITY INSPECTED 4

20000905 098

DISTRIBUTION STATEMENT A
Approved for Public Release
Distribution Unlimited

A Correlation between Flight-determined Lateral Derivatives and Ground-based Data for the Pilatus PC 9/A Training Aircraft in Cruise Configuration

Hilary A. Keating, Nick van Bronswijk, Andrew D. Snowden and Jan S. Drobik

Air Operations Division
Aeronautical and Maritime Research Laboratory

DSTO-TR-0988

ABSTRACT

A series of flight tests were conducted on the PC 9/A aircraft, A23-045, at the Royal Australian Air Force's Aircraft Research and Development Unit. System identification techniques were applied to the data obtained from these flight tests to determine the stability and control derivatives of the aircraft. The lateral results for the aircraft in cruise configuration are presented in this report and comparisons are made with empirical and ground based estimates.

APPROVED FOR PUBLIC RELEASE

DEPARTMENT OF DEFENCE
DEFENCE SCIENCE & TECHNOLOGY ORGANISATION

DSTO

AQF00-12-3798

DSTO-TR-0988

Published by

*DSTO Aeronautical and Maritime Research Laboratory
506 Lorimer St,
Fishermans Bend, Victoria, Australia 3207*

Telephone: (03) 9626 7000

Facsimile: (03) 9626 7999

© Commonwealth of Australia 2000

AR No. AR-011-475

June, 2000

APPROVED FOR PUBLIC RELEASE

A Correlation between Flight-determined Lateral Derivatives and Ground-based Data for the Pilatus PC 9/A Training Aircraft in Cruise Configuration

EXECUTIVE SUMMARY

Air Operations Division (AOD) has developed, or acquired, a number of fixed-wing flight dynamic models and is also responsible for providing advice to the Australian Defence Organisation (ADO) on flight simulator flight dynamic model requirements. The models generally make use of extensive static and dynamic stability and control derivative databases, in addition to engine and flight control models. The static model data may be obtained from wind tunnel testing, whilst the dynamic data is traditionally obtained from flight tests using system identification techniques.

The system identification techniques used to estimate aerodynamic derivatives of conventional aircraft are well established. The major requirement of these techniques is high fidelity measurements of manoeuvre input (i.e. control surface deflections), and aircraft response (i.e. angular rates and linear accelerations), as well as air data including airspeed, altitude, angle-of-attack and angle-of-sideslip.

Following the completion of the AOD PC 9/A wind tunnel tests, the requirement existed for a dedicated flight dynamic modelling flight test program to both validate the flight dynamic model of the PC 9/A and to provide dynamic derivative estimates which were unobtainable in the AMRL wind tunnel. An instrumentation suite, including an air data probe for the direct and accurate measurement of angle-of-attack, angle-of-sideslip, temperature, and static and dynamic pressure, was fitted to the aircraft and a test manoeuvre matrix was designed specifically for the purpose of gathering flight dynamic data. This flight test program was conducted at the Aircraft Research and Development Unit (ARDU) during 1998/99.

This report details the analysis of the lateral manoeuvres carried out with the aircraft in the cruise configuration. The static and dynamic derivatives thus obtained are compared with wind tunnel estimates as well as a number of empirical estimates obtained from alternative sources. A discussion of some of the difficulties encountered during the estimation process is also included. The data obtained from these tests will be used in the development of the PC 9/A flight dynamic model for the purpose of enhancing AOD support for the PC 9/A fleet, including possible upgrades to the part-task trainer.

DSTO-TR-0988

Authors



Hilary Keating
Air Operations Division

Hilary Keating graduated from the University of Sydney in 1998, having obtained a Bachelor of Engineering in Aeronautical Engineering with first class honours. She commenced employment at AMRL in 1999, and has been involved in performance modelling and parameter identification of the Pilatus PC 9/A.



Nick van Bronswijk
Air Operations Division

Nick van Bronswijk graduated from the University of Sydney with first class honours in Aeronautical Engineering in 1995. He is currently completing his PhD in the area of propeller power effects. Since joining AMRL in 1998 he has been involved with a range of projects including flight and wind tunnel test programs of the Pilatus PC 9/A.



Andrew Snowden
Air Operations Division

Andrew Snowden graduated from the Royal Melbourne Institute of Technology in 1991, having obtained a Bachelor of Engineering in Aerospace Engineering with first class honours. Before commencing work at AMRL he served a short term attachment with McDonnell Douglas in St. Louis, Missouri, as the recipient of the McDonnell Aircraft Company Aerospace Engineering Prize for 1991. He commenced employment at AMRL in 1992 and participated in several experimental investigations in a number of different fields during his rotation. Now a full time member of the flight dynamics and performance area of the Air Operations Division, his most recent work includes the organisation of flight testing for parameter identification of the Pilatus PC 9/A as well as performance estimation of modern jet fighters.

Jan Drobik

Air Operations Division



Jan Drobik leads a team that is responsible for the implementation of solutions to flight dynamic problems which arise throughout the ADF's fleet of aircraft. Since joining the then ARL in 1978, he has acquired broad experience in the areas of flight dynamics and experimental aerodynamics. He has been responsible for the development of aircraft flight dynamic models and aerodynamic parameter estimation techniques within AMRL, and has managed its successful application to a wide range of practical problems. He has been involved in TTCP activities in AER Technical Panel AER TP-5 for many years, becoming Australian National Leader in 1998.

Contents

Glossary		xi
Notation		xi
1 Introduction		1
2 PC 9/A Test Aircraft		1
2.1 Aircraft Description		1
2.2 Flight Control System		2
2.3 Weight, Centre-of-Gravity and Mass Moments-of-Inertia		2
3 Instrumentation		2
4 Methods of Analysis		3
4.1 Stepwise Regression		3
4.1.1 Error Band		4
4.2 Maximum Likelihood		4
4.2.1 Cramer-Rao Bounds		5
5 Results and Discussion		5
5.1 Angle-of-Sideslip Derivatives		5
5.2 Yaw Rate Derivatives		6
5.3 Roll Rate Derivatives		6
5.4 Control Derivative		7
5.5 Variation of Lateral Derivatives with Rate of Climb and Angle-of-Attack		7
5.6 Manoeuvre Type and Altitude Dependency		8
6 Conclusions		9
References		10

Appendices

A	Weight, Centre-of-Gravity and Mass Moments-of-Inertia	34
----------	--	-----------

B	Side Force, Rolling Moment and Yawing Moment Coefficients	36
B.1	Side Force Coefficient	36
B.2	Yawing Moment Coefficient	36
B.3	Rolling Moment Coefficient	36

Figures

1	Air data boom installation.	12
2	PC 9/A angle-of-sideslip derivatives, 3-2-1-1 manoeuvres at 5000 ft.	13
3	PC 9/A angle-of-sideslip derivatives, 3-2-1-1 manoeuvres at 10 000 ft.	14
4	PC 9/A angle-of-sideslip derivatives, 3-2-1-1 manoeuvres at 15 000 ft.	15
5	PC 9/A angle-of-sideslip derivatives, doublet manoeuvres at 5000 ft.	16
6	PC 9/A angle-of-sideslip derivatives, doublet manoeuvres at 15 000 ft.	17
7	PC 9/A yaw rate derivatives, 3-2-1-1 manoeuvres at 5000 ft.	18
8	PC 9/A yaw rate derivatives, 3-2-1-1 manoeuvres at 10 000 ft.	19
9	PC 9/A yaw rate derivatives, 3-2-1-1 manoeuvres at 15 000 ft.	20
10	PC 9/A yaw rate derivatives, doublet manoeuvres at 5000 ft.	21
11	PC 9/A yaw rate derivatives, doublet manoeuvres at 15 000 ft.	22
12	PC 9/A roll rate derivatives, 3-2-1-1 manoeuvres at 5000 ft.	23
13	PC 9/A roll rate derivatives, 3-2-1-1 manoeuvres at 10 000 ft.	24
14	PC 9/A roll rate derivatives, 3-2-1-1 manoeuvres at 15 000 ft.	25
15	PC 9/A roll rate derivatives, doublet manoeuvres at 5000 ft.	26
16	PC 9/A roll rate derivatives, doublet manoeuvres at 15 000 ft.	27
17	PC 9/A control derivatives, 3-2-1-1 manoeuvres at 5000 ft.	28
18	PC 9/A control derivatives, 3-2-1-1 manoeuvres at 10 000 ft.	29
19	PC 9/A control derivatives, 3-2-1-1 manoeuvres at 15 000 ft.	30
20	PC 9/A control derivatives, doublet manoeuvres at 5000 ft.	31
21	PC 9/A control derivatives, doublet manoeuvres at 15 000 ft.	32
22	Variation of lateral derivatives with nominal rate of climb.	33
B1	Relative magnitudes of C_Y equation components.	37
B2	Relative magnitudes of C_n equation components.	38
B3	Relative magnitudes of C_l equation components.	38

Tables

1	Lateral derivatives estimated	4
2	Summary of derivatives estimated using maximum likelihood	8
3	Summary of derivatives estimated by stepwise regression	8
A1	Flight test aircraft mass distribution [3, 4].	34

DSTO-TR-0988

Glossary

AHRS	Artificial Horizon Reference System
AMRL	Aeronautical and Maritime Research Laboratory
AOD	Air Operations Division
ARDU	Aircraft Research and Development Unit
DSTO	Defence Science and Technology Organisation
GDAS	General Data Acquisition System
IAS	Indicated Airspeed
ITT	Inlet Turbine Temperature
KIAS	Knots Indicated Airspeed
MAC	Mean Aerodynamic Chord
NASA	National Aeronautics and Space Administration
NG	Gas generator speed
OAT	Outside Air Temperature
PAP	Primary Analysis Processor
RAAF	Royal Australian Air Force
SHP	Shaft Horse Power

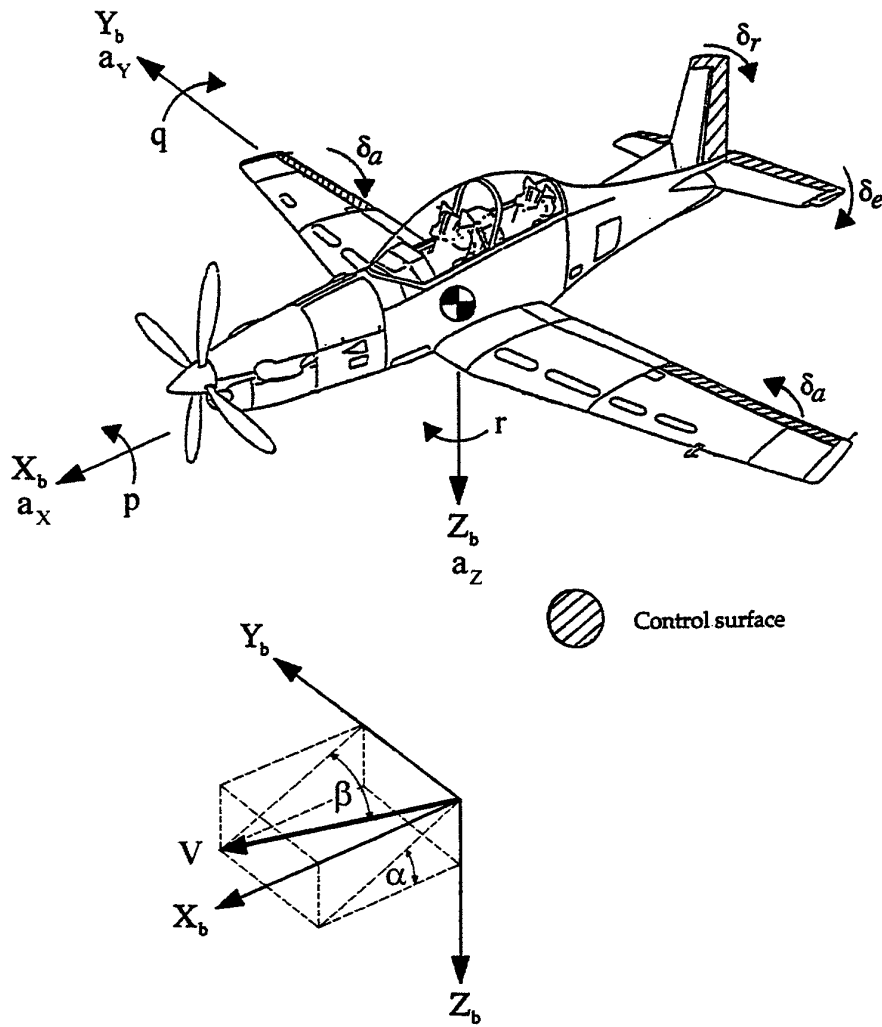
Notation

a_X, a_Y, a_Z	Body axes linear accelerations (g)
b	Reference span (10.124 m)
C_l	Rolling moment coefficient $C_l = \frac{l}{qSb}$
C_{l_β}	Rolling moment coefficient due to angle-of-sideslip $C_{l_\beta} = \frac{\partial C_l}{\partial \beta}$ (per degree)
C_{l_p}	Rolling moment coefficient due to roll rate $C_{l_p} = \frac{\partial C_l}{\partial (\frac{p}{2V})}$ (per radian)
C_{l_r}	Rolling moment coefficient due to yaw rate $C_{l_r} = \frac{\partial C_l}{\partial (\frac{r}{2V})}$ (per radian)
$C_{l_{\delta_a}}$	Rolling moment coefficient due to aileron deflection $C_{l_{\delta_a}} = \frac{\partial C_l}{\partial \delta_a}$ (per degree)
$C_{l_{\delta_r}}$	Rolling moment coefficient due to rudder deflection $C_{l_{\delta_r}} = \frac{\partial C_l}{\partial \delta_r}$ (per degree)
C_n	Yawing moment coefficient $C_n = \frac{n}{qSb}$
C_{n_β}	Yawing moment coefficient due to angle-of-sideslip $C_{n_\beta} = \frac{\partial C_n}{\partial \beta}$ (per degree)
C_{n_p}	Yawing moment coefficient due to roll rate $C_{n_p} = \frac{\partial C_n}{\partial (\frac{p}{2V})}$ (per radian)
C_{n_r}	Yawing moment coefficient due to yaw rate $C_{n_r} = \frac{\partial C_n}{\partial (\frac{r}{2V})}$ (per radian)
$C_{n_{\delta_a}}$	Yawing moment coefficient due to aileron deflection $C_{n_{\delta_a}} = \frac{\partial C_n}{\partial \delta_a}$ (per degree)
$C_{n_{\delta_r}}$	Yawing moment coefficient due to rudder deflection $C_{n_{\delta_r}} = \frac{\partial C_n}{\partial \delta_r}$ (per degree)
C_Y	Side force coefficient $C_Y = \frac{Y}{qS}$
C_{Y_β}	Side force coefficient due to angle-of-sideslip $C_{Y_\beta} = \frac{\partial C_Y}{\partial \beta}$ (per degree)
C_{Y_p}	Side force coefficient due to roll rate $C_{Y_p} = \frac{\partial C_Y}{\partial (\frac{p}{2V})}$ (per radian)
C_{Y_r}	Side force coefficient due to yaw rate $C_{Y_r} = \frac{\partial C_Y}{\partial (\frac{r}{2V})}$ (per radian)
$C_{Y_{\delta_a}}$	Side force coefficient due to aileron deflection $C_{Y_{\delta_a}} = \frac{\partial C_Y}{\partial \delta_a}$ (per degree)
$C_{Y_{\delta_r}}$	Side force coefficient due to rudder deflection $C_{Y_{\delta_r}} = \frac{\partial C_Y}{\partial \delta_r}$ (per degree)

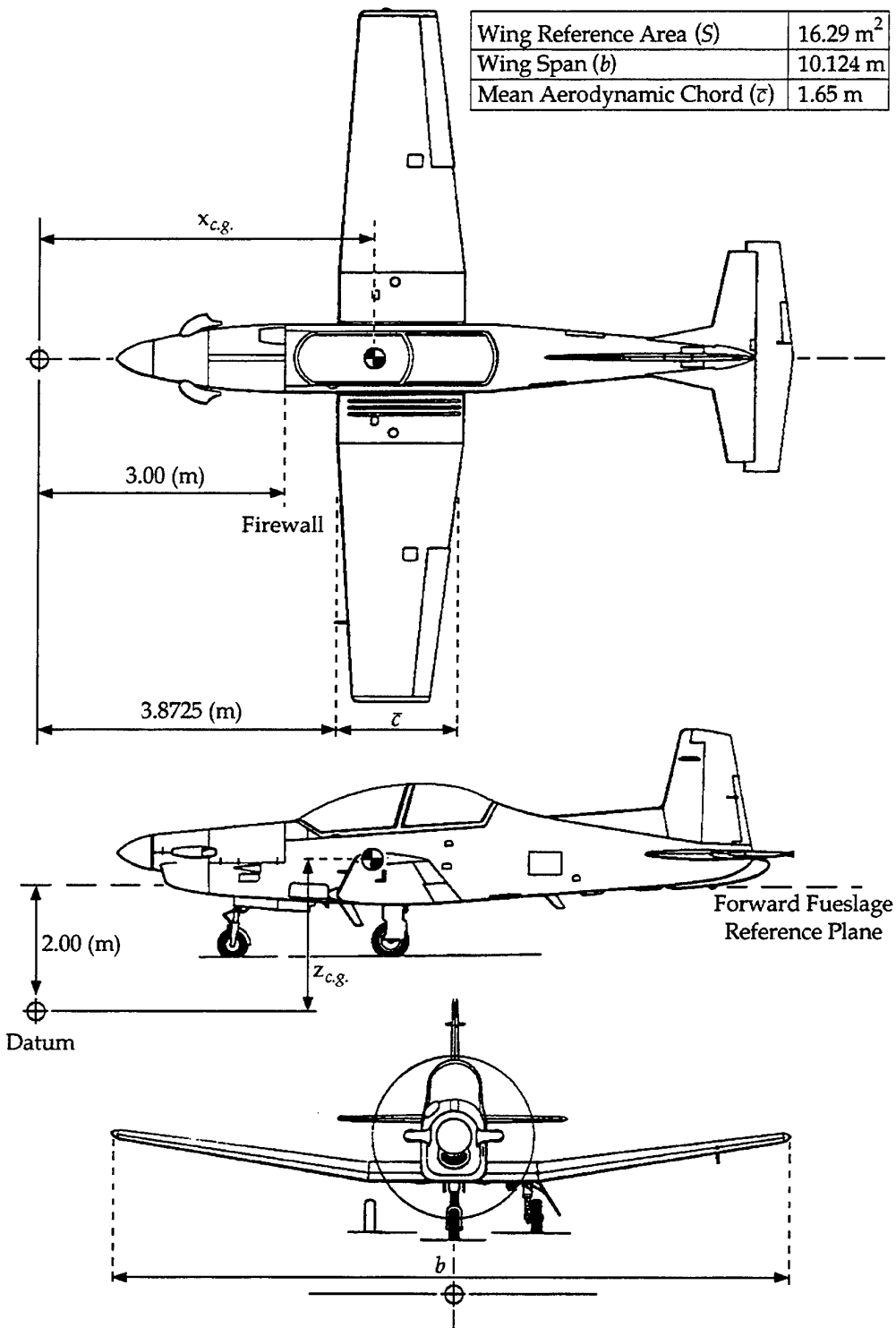
\bar{c}	Reference chord (1.65 m)
F	Ratio of the regression mean square to the residual mean square
g	Gravitational acceleration (9.81 m/s ²)
I_{XX}	Roll moment of inertia (kg.m ²)
I_{YY}	Pitch moment of inertia (kg.m ²)
I_{ZZ}	Yaw moment of inertia (kg.m ²)
I_{XY}	Cross product of moment of inertia (kg.m ²)
I_{XZ}	Cross product of moment of inertia (kg.m ²)
I_{YZ}	Cross product of moment of inertia (kg.m ²)
l	Rolling moment (N.m)
M	Mass of aircraft (kg)
n	Yawing moment (N.m)
p	Roll rate (rad/s)
q	Pitch rate (rad/s)
\bar{q}	Dynamic pressure (N/m ²)
R^2	Squared multiple correlation coefficient
r	Yaw rate (rad/s)
S	Reference area (16.29 m ²)
V	True velocity (m/s)
X	Longitudinal force (N)
$x_{c.g.}$	Longitudinal c.g. position (m)
Y	Side force (N)
$y_{c.g.}$	Lateral c.g. position (m)
Z	Vertical force (N)
$z_{c.g.}$	Vertical c.g. position (m)
α	Angle-of-attack (°)
β	Angle-of-sideslip (°)
δ_a	Aileron deflection ($\delta_a = \delta_{aL} - \delta_{aR}$) (°)
δ_e	Elevator deflection (°)
δ_r	Rudder deflection (°)
θ	Pitch angle (°)
ϕ	Roll angle (°)
ψ	Yaw angle (°)

Subscripts

b	Body axes
$c.g.$	Centre of gravity
F	Fuel
L	Left (port)
R	Right (starboard)



Aircraft sign convention and flow angle definitions (body axes).



Aircraft Principle Dimensions.
 (Numeric data sourced from Pilatus Structural Configuration Drawing 506.00.09.220F)

DSTO-TR-0988

1 Introduction

The Pilatus PC 9/A is one of a number of high performance turbo-prop aircraft currently operated by the Royal Australian Air Force (RAAF). Work currently underway in the Air Operations Division (AOD) of the Defence Science and Technology Organisation (DSTO) includes investigations into the propeller power effects of such aircraft, and the PC 9/A was considered a suitable platform for study. A six degree-of-freedom flight dynamic model of the PC 9/A has been developed by AOD for use in these investigations, as well as for pilot-in-the-loop simulations in the Air Operations Simulation Centre and incident and accident investigations.

The development of a flight dynamic model requires information on the static and dynamic stability and control derivatives of the aircraft, as well as flight control laws and physical properties. The static data for the PC 9/A were collected during both power-off and power-on testing of a scaled aircraft model in the Aeronautical and Maritime Research Laboratory (AMRL) low-speed wind tunnel. Additional power-off static data were obtained from a computational fluid dynamic model for a limited number of aircraft configurations.

Flight test data for the PC 9/A was required to both validate the flight dynamic model and to provide dynamic derivative estimates of the aircraft. A flight test program was conducted on a PC 9/A aircraft, serial number A23-045, by the RAAF Aircraft Research and Development Unit (ARDU) between November 1998 and February 1999. The details of this flight test program and the aircraft instrumentation are reported in reference [1]. The estimation of the stability and control derivatives from the flight test data involved the use of system identification techniques, and required control input, aircraft response and flight condition data, measured using a high fidelity instrumentation system. Maximum likelihood and stepwise regression techniques were employed for the system identification. The longitudinal derivatives for the PC 9/A aircraft in the cruise configuration determined using system identification techniques are reported in reference [2].

This report presents the lateral stability and control derivatives of the PC 9/A extracted from flight test data for the cruise configuration, including a comparison with AMRL wind tunnel test data and empirical results. Sections 2 and 3 present details of the test aircraft and instrumentation system. Section 4 presents the system identification techniques, while section 5 discusses the results.

2 PC 9/A Test Aircraft

2.1 Aircraft Description

The flight test aircraft, A23-045 is a Pilatus PC 9/A operated by ARDU. The PC 9/A is a single-engine, metal-skinned, low-wing, tandem two-seat training aircraft. The aircraft is powered by a Pratt and Whitney PT6A-62 turbo-prop engine flat rated to 950 SHP [3], which drives a Hartzell HC-D4N-2A four-blade variable pitch propeller. The aircraft was instrumented as outlined in section 3.

2.2 Flight Control System

The aircraft primary flight controls consist of the ailerons, rudder and elevator. The control surfaces are manually operated from a conventional dual control column and rudder pedal arrangement. The stick and rudder pedals are connected to the control surfaces through a system of control rods, bellcranks, cables and levers. Trimming control is provided on all three axes.

2.3 Weight, Centre-of-Gravity and Mass Moments-of-Inertia

The test aircraft, A23-045, was weighed by ARDU prior to the flight tests and had a basic mass of 1784.5 kg and a longitudinal centre-of-gravity position of 26.25% MAC [4]. During the flight test program, the aircraft weight, centre-of-gravity and mass moments-of-inertia varied with fuel usage. These parameters were calculated for each test manoeuvre using the equations in Appendix A.

3 Instrumentation

Aircraft A23-045 was fitted with an instrumentation system designed specifically for the gathering of flight dynamic data. A summary of the instrumentation used in the flight test program is included below and a more comprehensive description of the design requirements and calibration is included in references [1] and [5]. The ARDU General Data Acquisition System (GDAS) was fitted in place of the rear ejection seat. The data were encoded by a 16-bit pulse code modulation system and were recorded onboard the aircraft using a MARS-2000 14-track tape. Real-time flight test monitoring was provided by telemetry data transmitted to the ARDU Primary Analysis Processor (PAP) hut.

The angular rates (p, q, r) and linear accelerations (a_X, a_Y, a_Z) were measured using the ARDU KAISG1134-1 Motion Platform. This consisted of three Smith Industries 950 RGS angular rate gyros and three SunStrand QA1400 servo accelerometers. The aircraft roll, pitch and yaw attitude angles (ϕ, θ, ψ) were obtained by tapping output from the existing LISA 2000A Artificial Horizon Reference System (AHRS).

Static outside air temperature (OAT), indicated airspeed (IAS), angle-of-attack (α) and angle-of-sideslip (β) were obtained from the Rosemount Model 92AN flight test air data boom, mounted on the outboard hardpoint on the starboard wing (see figure 1). Aileron and elevator deflections were measured using Space Age Control Inc. series 160 cable position transducers. Rudder deflection was measured using a type 26V-11CX4C position transducer. All sensors were calibrated prior to commencement of the flight test program.

The aircraft was also instrumented to measure engine torque, propeller speed, inlet turbine temperature (ITT), gas generator speed (NG), fuel flow and fuel quantity. The torque, propeller speed, altitude and true airspeed, when used in conjunction with a performance map for the Hartzell HC-D4N-2A propeller [6], allowed the calculation of engine thrust.

4 Methods of Analysis

During the flight test program, doublet and 3-2-1-1 manoeuvres were performed about steady flight conditions at airspeeds between 90 and 200 KIAS. Reference [1] describes these manoeuvres in detail. The 26 lateral doublet and 129 lateral 3-2-1-1 manoeuvres were analysed using stepwise regression [7] and maximum likelihood estimation techniques [8] to determine the lateral stability and control derivatives of the aircraft.

A range of independent aircraft derivative data were used for comparison purposes and, for the maximum likelihood analysis, as *a priori* estimates to increase the rate of convergence of the system identification. This data was sourced from AMRL power-off wind tunnel tests [9] and empirical data estimated by the University of Sydney [10] using Datcom [11] and Pilatus [12] using both Digital Datcom [13] [14] and other 'long-hand' methods.

A right handed orthogonal axes system was adopted for the analysis of the flight test data. Positive control surface deflections were defined as elevator trailing edge down, rudder trailing edge to port, and starboard aileron trailing edge down, port aileron trailing edge up.

4.1 Stepwise Regression

Stepwise regression is an unbiased least squares estimator in which new independent variables are inserted into a model, one at a time, until the regression equation is deemed acceptable. The appropriateness of the model can be determined by examining a number of quantities including the squared multiple correlation coefficient and the F statistic. The squared multiple correlation coefficient, R^2 , gives a measure of the importance of each variable as it is inserted into the equation [7]; however, the improvement in R^2 due to the addition of new terms must have some real significance besides simply reflecting the inclusion of more terms. This can be determined by monitoring the F statistic, the ratio of the regression mean square to the residual mean square. The inclusion of any significant terms is generally accompanied by an increase in the F statistic and the best fit with the least number of parameters may be obtained by maximising F. Any variable which does not make a significant contribution is removed from the model, with the selection process continuing until no new variables remain to be inserted into the equation. Whilst stepwise regression gives estimates of the derivatives included in the regression equation, it also permits a suitable structure for the model to be determined. In addition, it provides an independent check on the data estimated using the maximum likelihood technique.

The stepwise regression technique was applied using code available in the MATLAB[®] Statistics Toolbox [15]. The following model equations were identified during the analysis.

$$C_Y = C_{Y_0} + C_{Y_\beta}\beta + C_{Y_{\delta_r}}\delta_r \quad (1)$$

$$C_n = C_{n_0} + C_{n_\beta}\beta + C_{n_p}\frac{pb}{2V} + C_{n_r}\frac{rb}{2V} + C_{n_{\delta_r}}\delta_r \quad (2)$$

$$C_l = C_{l_0} + C_{l_\beta} \beta + C_{l_p} \frac{pb}{2V} + C_{l_r} \frac{rb}{2V} + C_{l_{\delta_a}} \delta_a \quad (3)$$

4.1.1 Error Band

Included in the stepwise regression analysis is the calculation of an error band on the estimated derivatives. For a confidence interval of 95%, this error band is approximately equal to two standard deviations. Figures 2 to 21 show the stepwise regression derivative estimates, including the calculated error band.

4.2 Maximum Likelihood

The maximum likelihood estimation technique was applied using the computer program, pEst, developed at NASA Dryden Flight Research Center [16]. pEst is an interactive parameter estimation program which solves a vector set of time-varying, ordinary differential equations of motion.

Prior to the application of the maximum likelihood technique, stepwise regression was used to determine a suitable structure for the lateral model equations. Those derivatives that were found to be statistically insignificant were not estimated using pEst. However, unlike stepwise regression, these derivatives were not removed from the model equations but were instead fixed at their *a priori* values. C_{Y_p} was fixed at a value of -0.16 (per radian), C_{Y_r} at 0.34 (per radian), $C_{Y_{\delta_a}}$ at 0.0 (per degree), $C_{n_{\delta_a}}$ at -0.000035 (per degree) and $C_{l_{\delta_r}}$ fixed at 0.00035 (per degree). These *a priori* values were obtained from empirical data of references [10] and [12]. The lateral derivatives which were identified using the maximum likelihood technique are given in table 1.

	Side Force	Yawing Moment	Rolling Moment
Aerodynamic	C_{Y_β}	C_{n_β}	C_{l_β}
	-	C_{n_p}	C_{l_p}
	-	C_{n_r}	C_{l_r}
Control	-	-	$C_{l_{\delta_a}}$
	$C_{Y_{\delta_r}}$	$C_{n_{\delta_r}}$	-

Table 1: Lateral derivatives estimated

The resulting total force and moment coefficient equations used in the state and response equations for the maximum likelihood analysis of the PC 9/A are given in equations 4, 5 and 6. The differences between equations 1, 2 and 3, and 4, 5 and 6 are important, and arise from the inclusion of the *a priori* values in the maximum likelihood technique.

$$C_Y = C_{Y_0} + C_{Y_\beta} \beta - 0.16 \frac{pb}{2V} + 0.34 \frac{rb}{2V} + C_{Y_{\delta_r}} \delta_r \quad (4)$$

$$C_n = C_{n_0} + C_{n_\beta}\beta + C_{n_p}\frac{pb}{2V} + C_{n_r}\frac{rb}{2V} - 0.000035\delta_a + C_{n_{\delta_r}}\delta_r \quad (5)$$

$$C_l = C_{l_0} + C_{l_\beta}\beta + C_{l_p}\frac{pb}{2V} + C_{l_r}\frac{rb}{2V} + C_{l_{\delta_a}}\delta_a + 0.00035\delta_r \quad (6)$$

4.2.1 Cramer-Rao Bounds

For the estimated parameters, pEst calculates a measure of the estimation certainty known as the Cramer-Rao bound. A detailed interpretation of this quantity is given in [17]. The Cramer-Rao bounds are shown for each derivative estimated by pEst in figures 2 to 21. The Cramer-Rao bounds have been factored in accordance with the procedures described in [17] to account for the presence of band-limited noise.

5 Results and Discussion

Lateral derivatives estimated via maximum likelihood parameter estimation, stepwise regression, empirical methods and power-off wind tunnel experiments are summarised in figures 2 to 21.

5.1 Angle-of-Sideslip Derivatives

Figures 2 to 6 show the angle-of-sideslip derivatives C_{Y_β} , C_{n_β} and C_{l_β} plotted against α . The flight test estimates of the side force due to angle-of-sideslip derivative, C_{Y_β} , generally fall between the empirical and wind tunnel estimates with the results showing a small degree of scatter at angles-of-attack above 6° . The estimates of C_{Y_β} from the stepwise regression method are slightly smaller in magnitude than those from the maximum likelihood technique.

Estimates of the directional stability derivative, C_{n_β} , show good agreement between results from stepwise regression and maximum likelihood techniques for both 3-2-1-1 and doublet manoeuvres. However, at low angles-of-attack, the flight test estimates are smaller than the wind tunnel and empirical estimates, which are both power-off. This difference is due to the imbalance between two competing effects acting on the portion of the vertical tail within the propeller slipstream, these being the increased dynamic pressure and the decreased angle of incidence. The reduction in angle of incidence dominates, resulting in an overall reduction in the directional stability of the aircraft. The flight test results show less variation with angle-of-attack than the wind tunnel results because the natural reduction in directional stability with angle-of-attack is partially balanced by the increasing portion of the vertical tail which is subject to increased dynamic pressure within the slipstream. In general, the Cramer-Rao bounds and stepwise regression error bands for C_{n_β} estimates are small.

The maximum likelihood and stepwise regression estimates of the rolling moment due to angle-of-sideslip derivative, C_{l_β} , show good agreement with the empirical and wind tunnel estimates for both the 3-2-1-1 and doublet manoeuvres. The flight test estimates of C_{l_β} show little variation with angle-of-attack, as predicted by the wind tunnel results. Similarly to C_{Y_β} estimates, C_{l_β} estimates from the stepwise regression technique are slightly smaller in magnitude than those obtained by the maximum likelihood technique.

5.2 Yaw Rate Derivatives

Figures 7 to 11 show the yaw rate derivatives, C_{n_r} and C_{l_r} , plotted against α . Angular rates were not measured during the wind tunnel test program and hence no wind tunnel yaw rate derivatives are available for comparison. As mentioned previously, C_{Y_r} was constrained to its *a priori* value for the maximum likelihood analysis, and not estimated in the stepwise regression analysis. Investigations were undertaken to assess the relative contribution of each derivative to the aircraft's forces and moments to ensure that those set to their *a priori* values were small contributors. This analysis, which is detailed in Appendix B, showed the yaw rate contribution to side force to be small.

The flight test estimates of the yawing moment due to yaw rate, C_{n_r} , agree well with the empirical estimate for both the 3-2-1-1 and doublet manoeuvres. A high degree of scatter is shown in the derivative estimates above 6° angle-of-attack. The stepwise regression technique gives estimates of C_{n_r} which are slightly larger in magnitude than the estimates from the maximum likelihood technique.

The rolling moment due to yaw rate, C_{l_r} , whilst being small is an important lateral-directional cross-coupling derivative. The flight test analysis results show C_{l_r} estimates to be generally larger than the empirical estimate for both 3-2-1-1 and doublet manoeuvres at all angles-of-attack. The flight test estimates of C_{l_r} show an increase with angle-of-attack. This is an expected result caused by the increase in lift coefficient with increasing angle-of-attack, which results in a greater rolling moment as the aircraft yaws (refer [18]). The flight test results show a small degree of scatter, particularly for the estimates obtained by the maximum likelihood technique.

5.3 Roll Rate Derivatives

The roll rate derivative estimates, C_{n_p} and C_{l_p} , are plotted against α in figures 12 to 16. The side force due to roll rate, C_{Y_p} , is a small derivative, not estimated in the stepwise regression or maximum likelihood analysis.

The yawing moment due to roll rate is an important lateral-directional cross-coupling derivative. The maximum likelihood estimates of C_{n_p} agree well with the stepwise regression estimates, and estimates from both techniques have small uncertainty levels. However, the flight test estimates are larger in magnitude than the empirical estimate. Similarly to C_{l_r} , C_{n_p} is influenced by the angle-of-attack and lift coefficient and its value is expected to vary with angle-of-attack [18]. This trend is seen in the flight test estimates, which show the value of C_{n_p} to decrease with angle-of-attack. The results also show a small degree of

scatter at angles-of-attack above 6° .

The roll damping derivative, C_{l_p} , estimates from both the stepwise regression and maximum likelihood techniques show good agreement with the empirical estimate. As expected [18], the C_{l_p} estimates do not show any variation with angle-of-attack. The results display little scatter with small error bands, indicating a high level of confidence in the results.

5.4 Control Derivative

The control derivatives estimates, $C_{Y_{\delta_r}}$, $C_{n_{\delta_r}}$ and $C_{l_{\delta_a}}$, are plotted against α in figures 17 to 21. The yawing moment due to aileron derivative, $C_{n_{\delta_a}}$, and rolling moment due to rudder derivative, $C_{l_{\delta_r}}$, are both small derivatives, which were not estimated in either the stepwise regression or maximum likelihood analysis.

Estimates of the side force due to rudder deflection derivative, $C_{Y_{\delta_r}}$, are scattered about the empirical and wind tunnel estimates. The maximum likelihood estimates of $C_{Y_{\delta_r}}$ have large Cramer-Rao bounds indicating a higher level of uncertainty in the estimates than other derivatives. However, $C_{Y_{\delta_r}}$ has only a small contribution to the total aircraft side force coefficient (refer Appendix B) and hence, the increased uncertainty in this derivative will not significantly affect the overall aircraft model characteristics.

Estimates of the rudder control effectiveness, $C_{n_{\delta_r}}$, show good agreement with the empirical and wind tunnel estimates and small uncertainty levels, particularly at low angles-of-attack. The flight test estimates of the aileron control effectiveness derivative, $C_{l_{\delta_a}}$, fall between the empirical and wind tunnel estimates for the 3-2-1-1 and doublet manoeuvres. These results exhibit only a small degree of scatter and show a good correlation between the stepwise regression and maximum likelihood estimation techniques.

5.5 Variation of Lateral Derivatives with Rate of Climb and Angle-of-Attack

The variation of lateral derivatives with angle-of-attack and nominal rate of climb for a selection of 3-2-1-1 manoeuvres is shown in figure 22. A linear curve fit was applied to each rate of climb data set to highlight the trends shown by the data. The influence of rate of climb with increasing angle-of-attack is seen in figure 22, with $C_{n_{\delta_r}}$, $C_{Y_{\beta}}$ and $C_{n_{\beta}}$ all increasing in magnitude. These trends are due to increases in the aircraft thrust coefficient and the dynamic pressure in the propeller slipstream as the rate of climb increases for a given angle-of-attack. These trends are supported by previous theoretical and experimental studies detailed in references [19] and [20]. For the manoeuvres in figure 22, thrust coefficient varies from approximately 0.02 to approximately 0.12.

5.6 Manoeuvre Type and Altitude Dependency

Tables 2 and 3 show the mean values across the linear angle-of-attack range ($0^\circ - 6^\circ$) of the aerodynamic derivatives estimated by both maximum likelihood and stepwise regression techniques, for each manoeuvre type and altitude band.

	3-2-1-1 5000 ft	3-2-1-1 10 000 ft	3-2-1-1 15 000 ft	Doublet 5000 ft	Doublet 15 000 ft
C_{Y_β}	-1.35E-02	-1.35E-02	-1.40E-02	-1.40E-02	-1.38E-02
$C_{Y_{\delta_r}}$	3.29E-03	3.00E-03	3.26E-03	3.27E-03	3.63E-03
C_{n_β}	1.41E-03	1.39E-03	1.33E-03	1.44E-03	1.42E-03
C_{n_p}	-6.32E-02	-6.29E-02	-5.28E-02	-5.40E-02	-6.06E-02
C_{n_r}	-2.01E-01	-1.97E-01	-2.03E-01	-1.80E-01	-1.91E-01
$C_{n_{\delta_r}}$	-2.02E-03	-1.91E-03	-1.89E-03	-1.73E-03	-1.86E-03
C_{l_β}	-1.52E-03	-1.55E-03	-1.49E-03	-1.37E-03	-1.36E-03
C_{l_p}	-5.08E-01	-5.04E-01	-4.94E-01	-4.64E-01	-4.77E-01
C_{l_r}	1.14E-01	1.20E-01	0.962E-01	1.31E-01	1.52E-01
$C_{l_{\delta_n}}$	-1.89E-03	-1.91E-03	-1.79E-03	-1.48E-03	-1.71E-03

Table 2: Summary of derivatives estimated using maximum likelihood

	3-2-1-1 5000 ft	3-2-1-1 10 000 ft	3-2-1-1 15 000 ft	Doublet 5000 ft	Doublet 15 000 ft
C_{Y_β}	-1.26E-02	-1.32E-02	-1.24E-02	-1.25E-02	-1.27E-02
$C_{Y_{\delta_r}}$	3.41E-03	3.50E-03	3.34E-03	3.45E-03	3.68E-03
C_{n_β}	1.45E-03	1.47E-03	1.45E-03	1.52E-03	1.50E-03
C_{n_p}	-5.54E-02	-5.21E-02	-5.19E-02	-4.72E-02	-5.55E-02
C_{n_r}	-2.43E-01	-2.23E-01	-2.24E-01	-2.19E-01	-2.28E-01
$C_{n_{\delta_r}}$	-1.99E-03	-1.91E-03	-1.91E-03	-1.87E-03	-1.88E-03
C_{l_β}	-1.38E-03	-1.28E-03	-1.37E-03	-1.34E-03	-1.30E-03
C_{l_p}	-4.89E-01	-4.44E-01	-4.66E-01	-4.38E-01	-4.61E-01
C_{l_r}	1.43E-01	1.43E-01	1.57E-01	1.47E-01	1.63E-01
$C_{l_{\delta_n}}$	-1.82E-03	-1.65E-03	-1.73E-03	-1.61E-03	-1.70E-03

Table 3: Summary of derivatives estimated by stepwise regression

The flight test derivative estimates from the 3-2-1-1 and doublet manoeuvres show similar trends for all lateral derivatives. In general, there was no significant change in uncertainty levels, derivative values or degree of scatter in the results for the two manoeuvre types at angles-of-attack below 6° . As no doublet manoeuvres were performed above this angle-of-attack, no conclusions can be drawn as to the influence of manoeuvre type on derivative estimates at higher angles-of-attack. As expected, figures 2 to 21 do not show any significant altitude dependency as the results are non-dimensionalised by dynamic pressure.

6 Conclusions

The lateral stability and control derivatives of the PC 9/A in the cruise configuration have been determined from flight test data measurements using maximum likelihood and stepwise regression estimation techniques. Comparisons have been made with derivative estimates from empirical methods and wind-tunnel experiments.

The sideslip derivatives, C_{Y_β} and C_{l_β} , showed good agreement between the flight test and ground-based estimates, while the results for C_{n_β} showed small differences due to the exclusion of power effects in the wind tunnel and empirical estimates. Flight test estimates of the yaw rate derivatives, C_{n_r} and C_{l_r} , showed good results when compared to empirical estimates, and displayed the expected trends with angle-of-attack. Estimates of C_{n_p} were slightly larger in magnitude than the empirical estimate, while flight test and empirical estimates of C_{l_p} compared well.

The control derivatives, $C_{Y_{\delta_r}}$, $C_{n_{\delta_r}}$ and $C_{l_{\delta_a}}$, were also estimated from the PC 9/A flight test measurements. $C_{n_{\delta_r}}$ and $C_{l_{\delta_a}}$ derivative estimates compared well with results estimated from empirical methods and wind tunnel experiments, while $C_{Y_{\delta_r}}$ estimates showed a higher level of uncertainty than other derivatives.

Trends were found in the $C_{n_{\delta_r}}$, C_{Y_β} and C_{n_β} estimates when plotted as a function of airspeed and rate of climb that agree with predictions from previous theoretical and experimental studies. In general, the flight test results did not show any significant variation with altitude or manoeuvre type.

References

1. A. D. Snowden. PC 9/A flight tests summary. Client Report AOD 99/01, Aeronautical and Maritime Research Laboratory, 1999.
2. A. D. Snowden, H. A. Keating, N. van Bronswijk, and J. S. Drobik. A correlation between flight-determined longitudinal derivatives and ground-based data for the Pilatus PC 9/A training aircraft in cruise configuration. Technical Report 0937, DSTO Aeronautical and Maritime Research Laboratory, Melbourne, Victoria, Australia, 2000.
3. Royal Australian Air Force. *Flight Manual PC 9/A. Defence Instruction (Air Force) AAP 7212.007-1*, June 1989.
4. M.C. Sciberras. Aircraft weigh record - A23-045. ARDU 2501/60/TechPt1(5), November 1998.
5. B. A. Woodyatt, A. D. Snowden, and K. E. Lillingston. The development of a PC 9/A flight dynamic model validation flight test program. Client Report AOD 98/07, Aeronautical and Maritime Research Laboratory, 1998.
6. British Aerospace. Pilatus PC 9/A performance maps. Technical memorandum, British Aerospace Aerodynamics, Brough.
7. V. Klein. Estimation of aircraft aerodynamic parameters from flight data. *Progress in Aerospace Sciences*, 26:1-77, 1989.
8. R.E. Maine and K.W. Iliff. Application of parameter estimation to aircraft stability and control, the output error approach. Reference Publication 1168, NASA Dryden Flight Research Facility, Edwards, California, USA, June 1986.
9. R. M. Carmichael and B. A. Woodyatt. Estimates of the power-off aerodynamic characteristics of the Pilatus PC 9/A. Client Report AOD 96/29, Aeronautical and Maritime Research Laboratory, February 1997.
10. N. van Bronswijk. *Investigation of the Effects of Propeller Power on the Stability and Control of a Propeller Powered, Single-Engined, Low-Wing Monoplane*. PhD thesis, University of Sydney, In Preparation.
11. R. D. Finck, editor. *U.S.A.F. Stability and Control DATCOM*. Engineering Documents, A Division of Information Handling Services, 1978.
12. PEI Aerodynamics. Evaluation of stability derivatives for the PC 9/A turbo-trainer. Technical report, Pilatus Aircraft Limited, 30 July 1983.
13. J.E. Williams and Vukelich. The USAF stability and control digital DATCOM - volume I, users manual. Technical Report AFFDL-TR-76-45, Vol I, McDonnell Douglas Astronautics Company - East, St Louis, Missouri, USA, November 1976.
14. J.E. Williams and Vukelich. The USAF stability and control digital DATCOM - volume II, implementation of DATCOM methods. Technical Report AFFDL-TR-76-45, Vol II, McDonnell Douglas Astronautics Company - East, St Louis, Missouri, USA, November 1976.

15. The MathWorks, *Statistics Toolbox User's Guide*, Inc, Natick, MA, January 1997.
16. J.E. Murray and R.E. Maine. pEst version 2.1 user's manual. Technical Memorandum 8828, NASA Ames Research Center, Dryden Flight Research Facility, Edwards, CA, USA, September 1987.
17. R.E. Maine and K.W. Iliff. User's manual for MMLE3, a general FORTRAN program for maximum likelihood parameter estimation. Technical Paper 1563, Dryden Flight Research Center, Edwards, California, USA, 1980.
18. B. Etkin. *Dynamics of Atmospheric Flight*. John Wiley & Sons Inc., 1972.
19. J. P. Shivers, M. P. Fink, and G. M. Ware. Full-scale wind tunnel investigation of the static longitudinal and lateral characteristics of a light single-engine low-wing airplane. TN D-5857, National Aeronautics and Space Administration, June 1970.
20. N. van Bronswijk, P. W. Gibbens, D. M. Newman, and K. C. Wong. Investigation of the effects of propeller power on the stability and control of a tractor-propeller powered single-engined low-wing monoplane. Technical Report 9801, University of Sydney, January 1998.

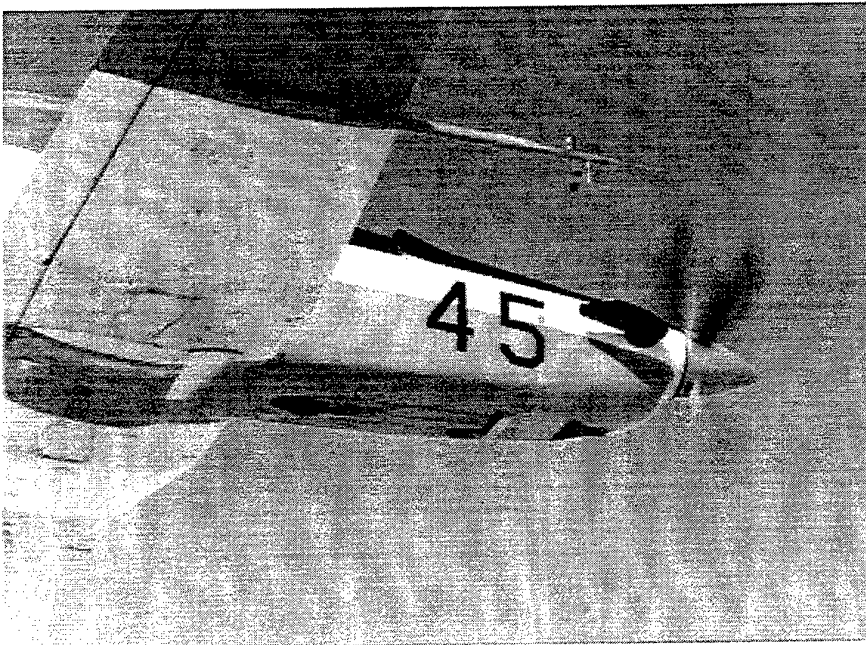


Figure 1: Air data boom installation.

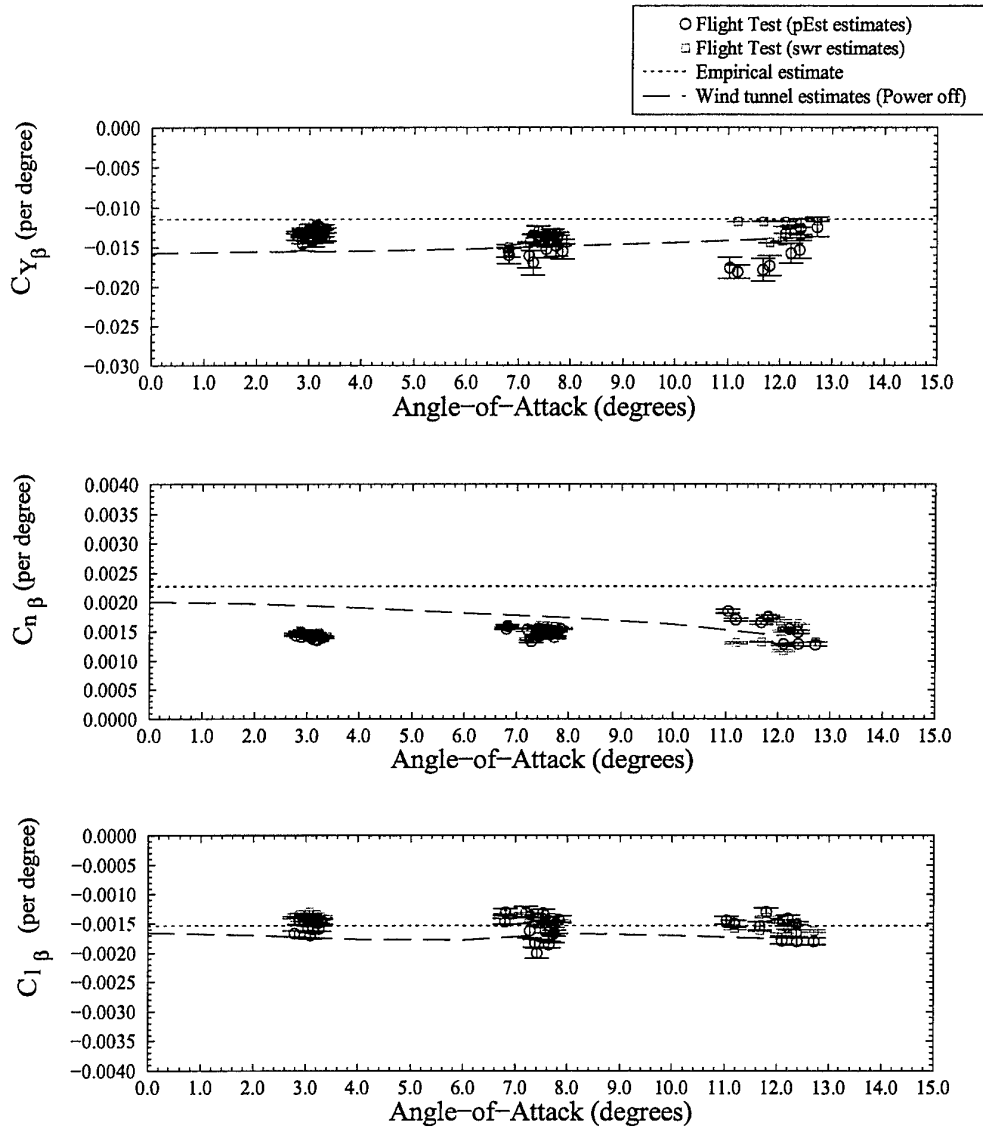


Figure 2: PC 9/A angle-of-sideslip derivatives, 3-2-1-1 manoeuvres at 5000 ft.

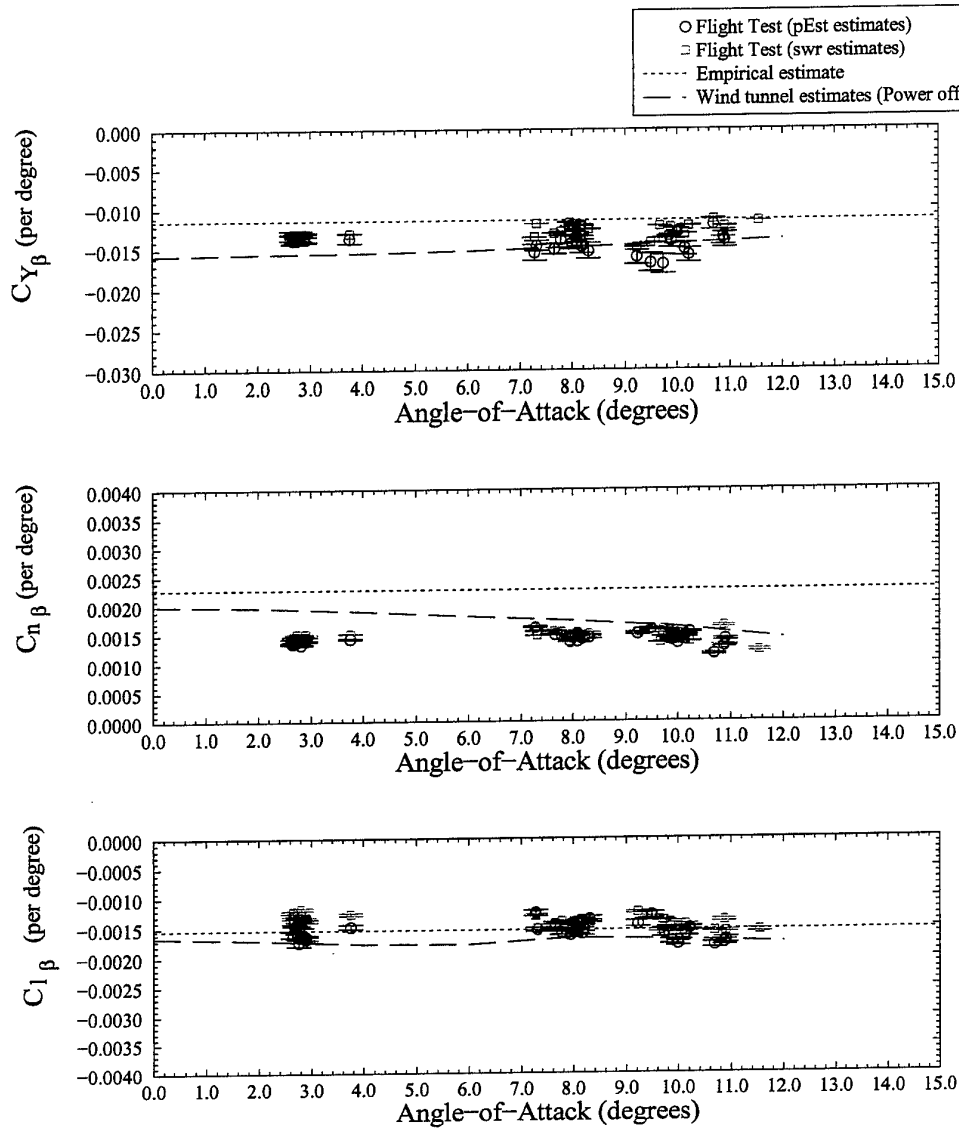


Figure 3: PC 9/A angle-of-sideslip derivatives, 3-2-1-1 manoeuvres at 10 000 ft.

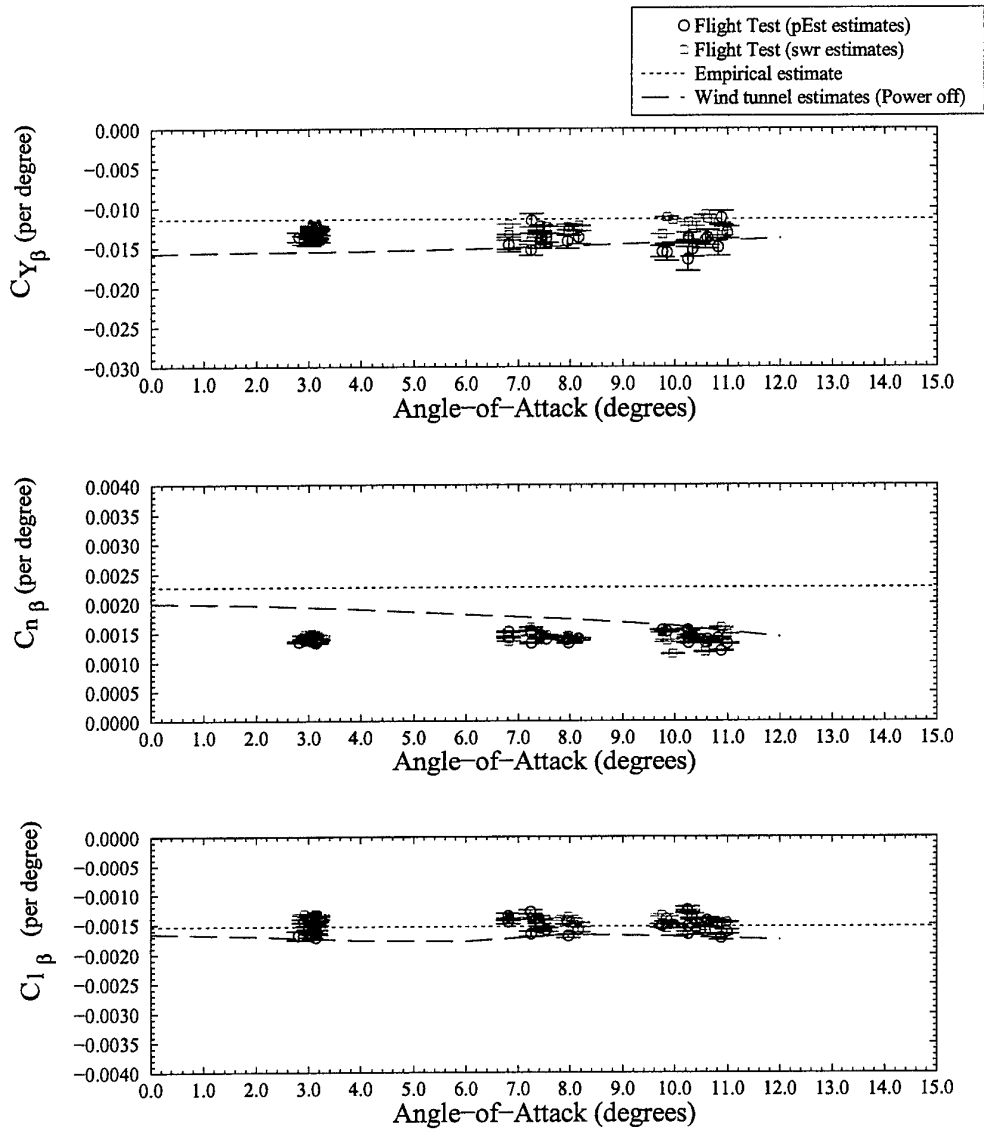


Figure 4: PC 9/A angle-of-sidslip derivatives, 3-2-1-1 manoeuvres at 15 000 ft.

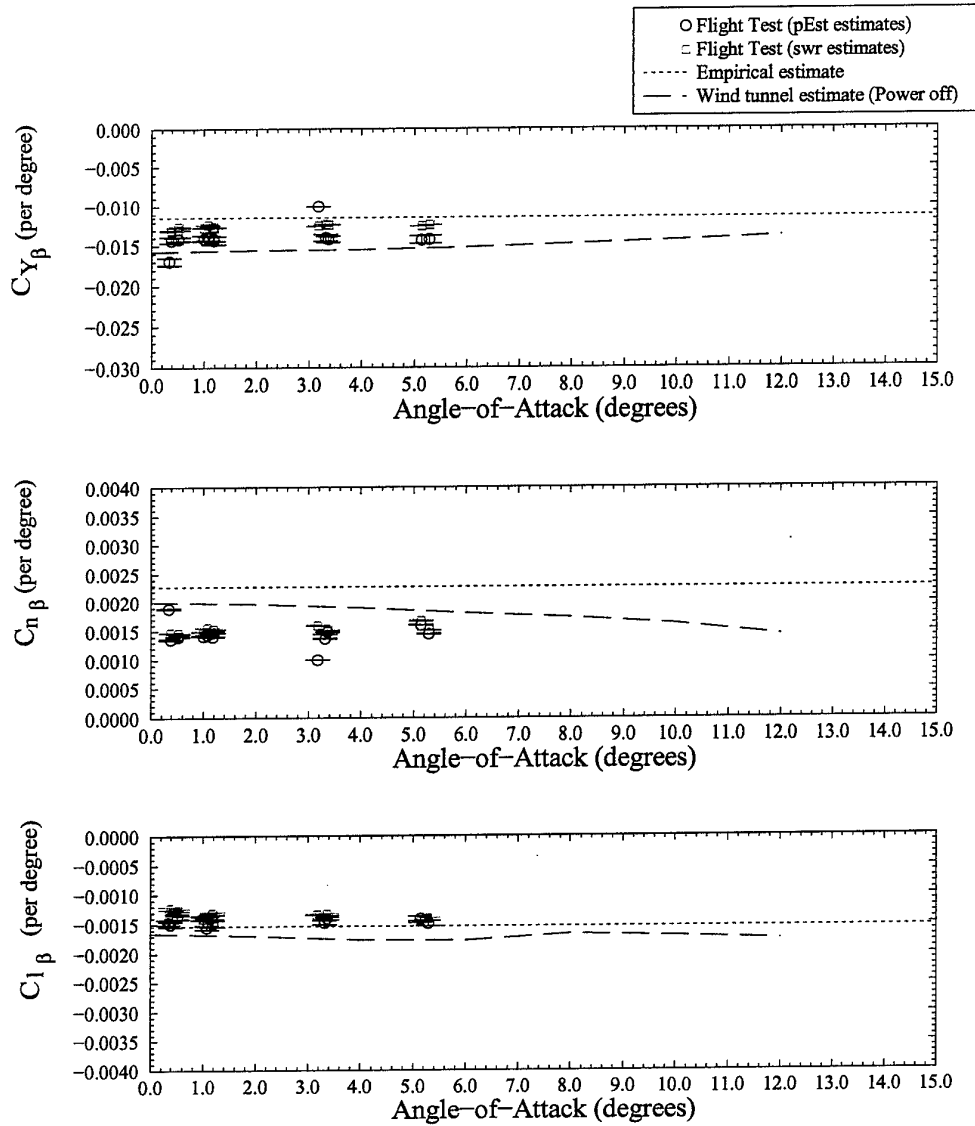


Figure 5: PC 9/A angle-of-sidslip derivatives, doublet manoeuvres at 5000 ft.

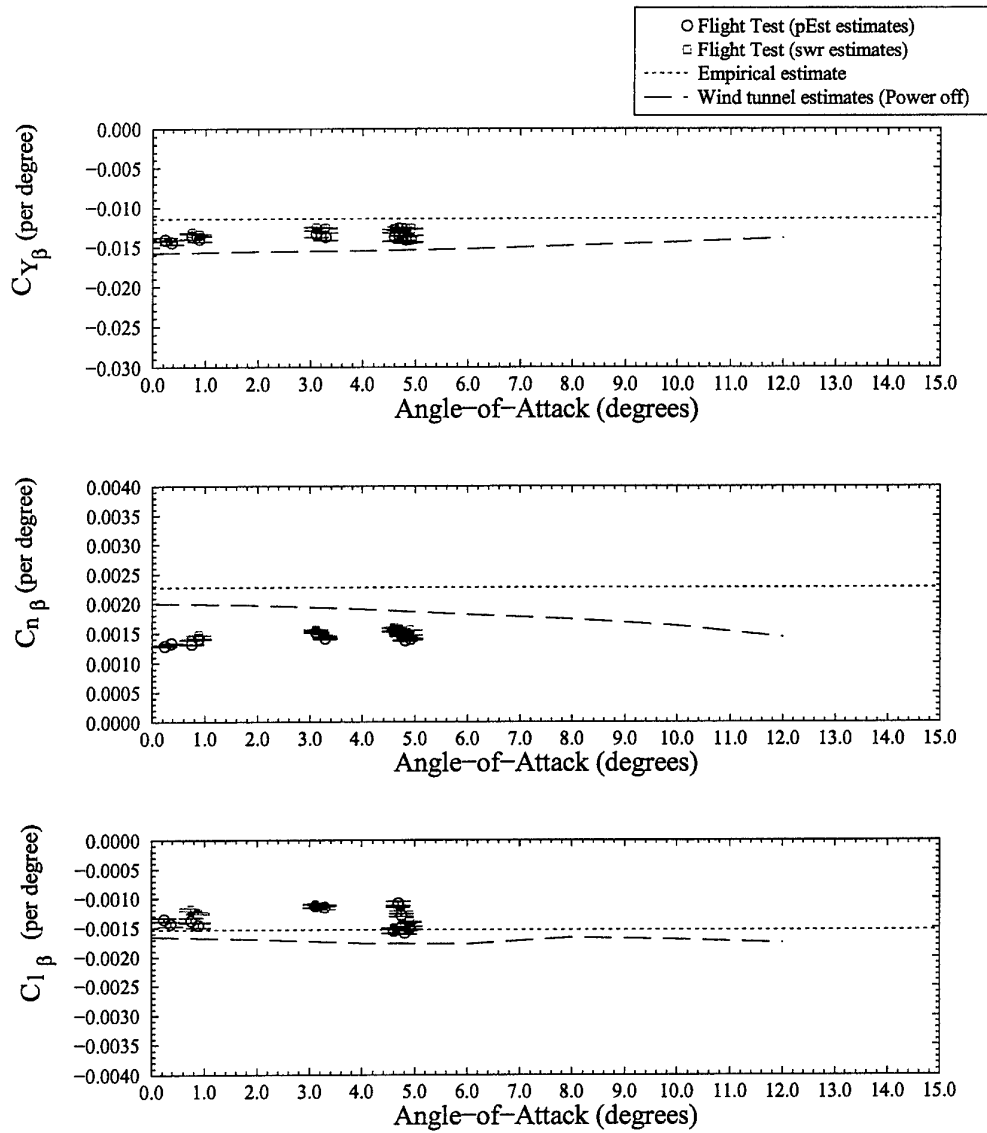


Figure 6: PC 9/A angle-of-sideslip derivatives, doublet manoeuvres at 15 000 ft.

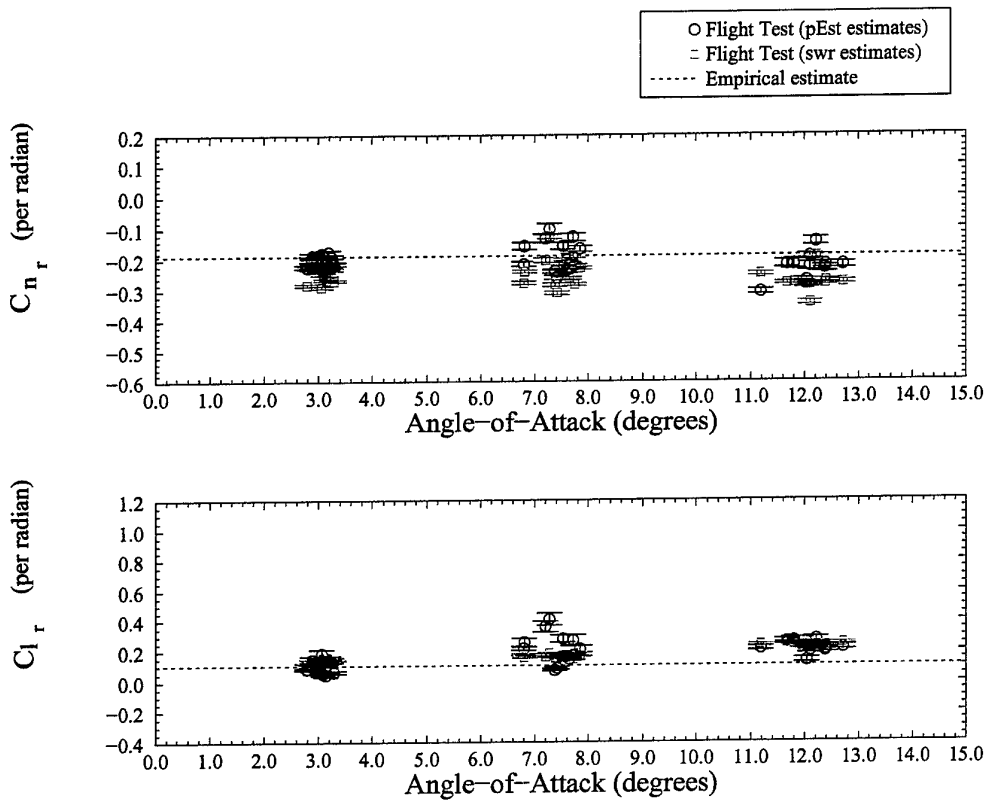


Figure 7: PC 9/A yaw rate derivatives, 3-2-1-1 manoeuvres at 5000 ft.

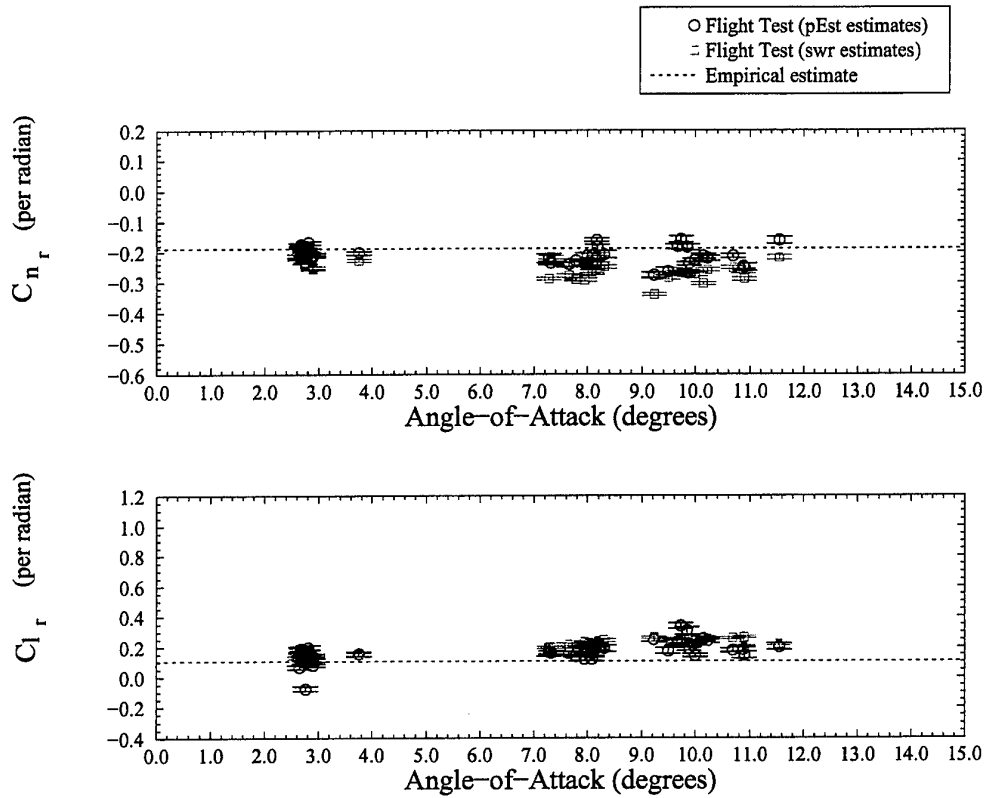


Figure 8: PC 9/A yaw rate derivatives, 3-2-1 manoeuvres at 10 000 ft.

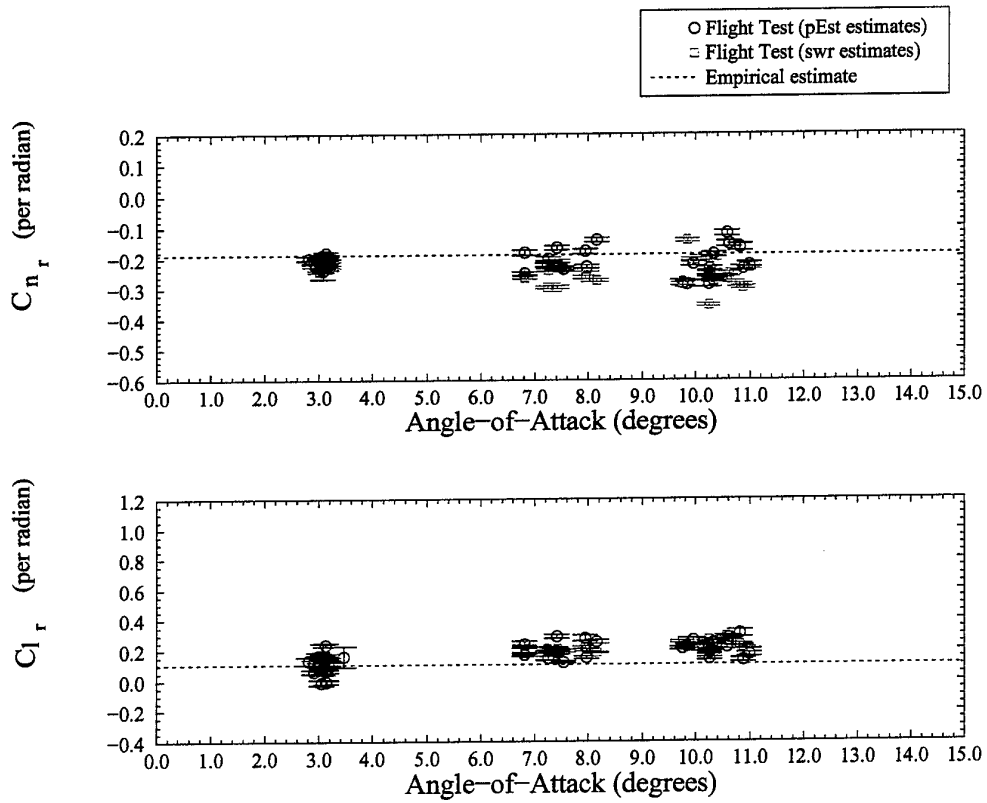


Figure 9: PC 9/A yaw rate derivatives, 3-2-1-1 manoeuvres at 15 000 ft.

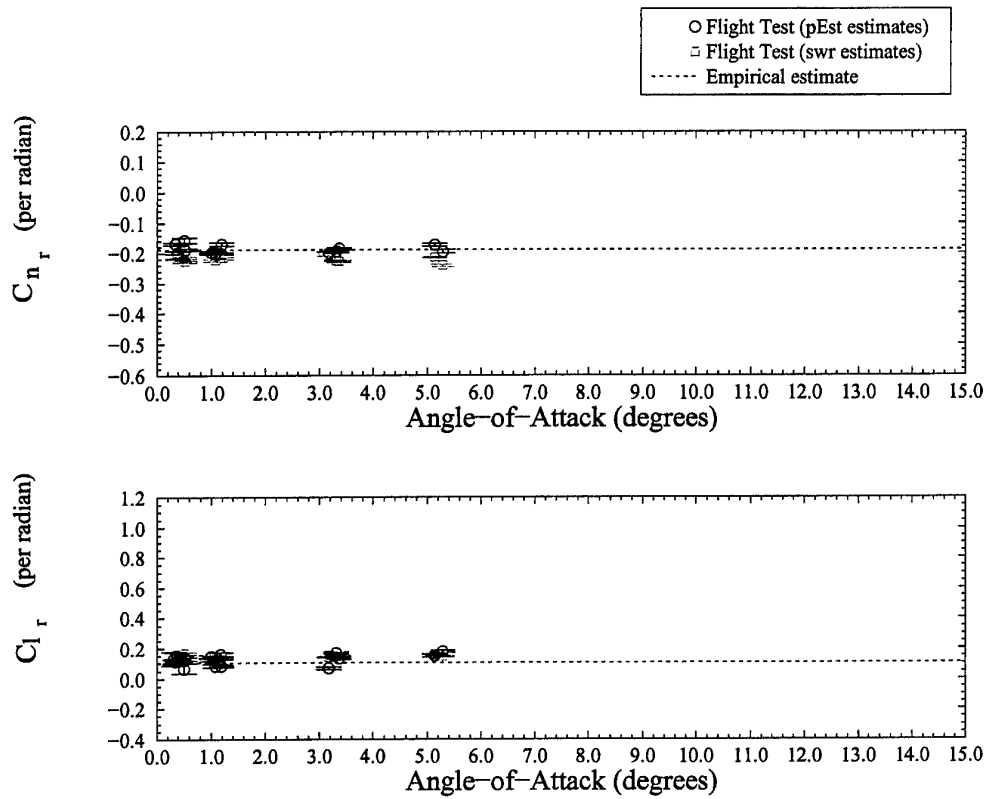


Figure 10: PC 9/A yaw rate derivatives, doublet manoeuvres at 5000 ft.

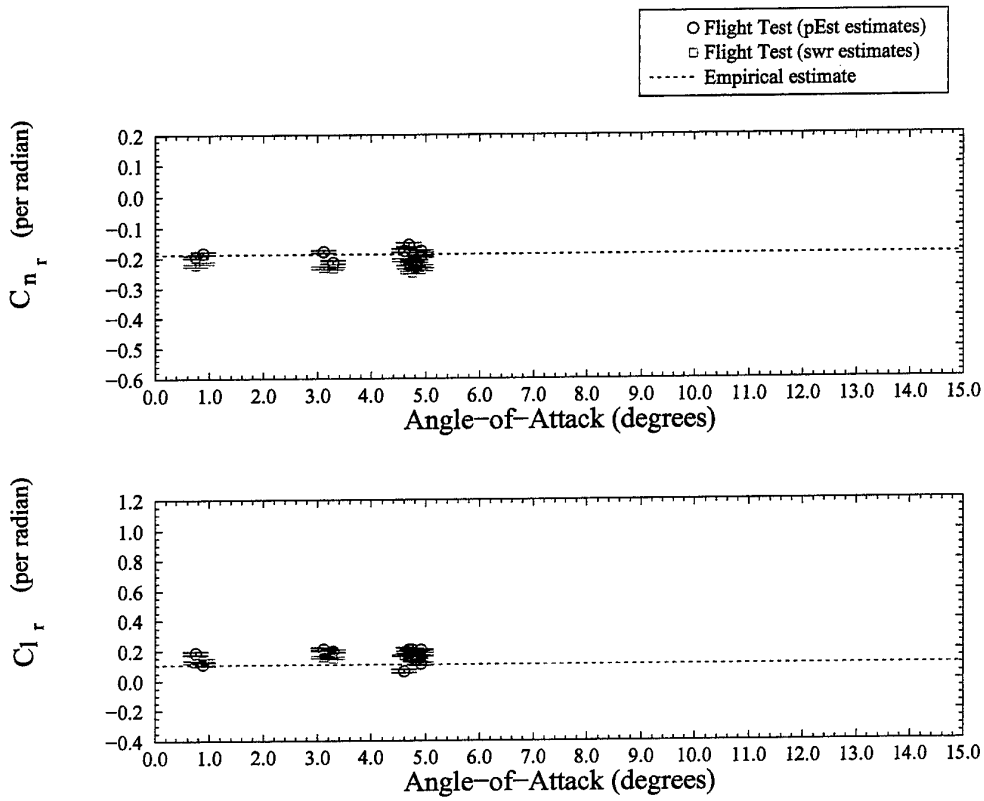


Figure 11: PC 9/A yaw rate derivatives, doublet manoeuvres at 15 000 ft.

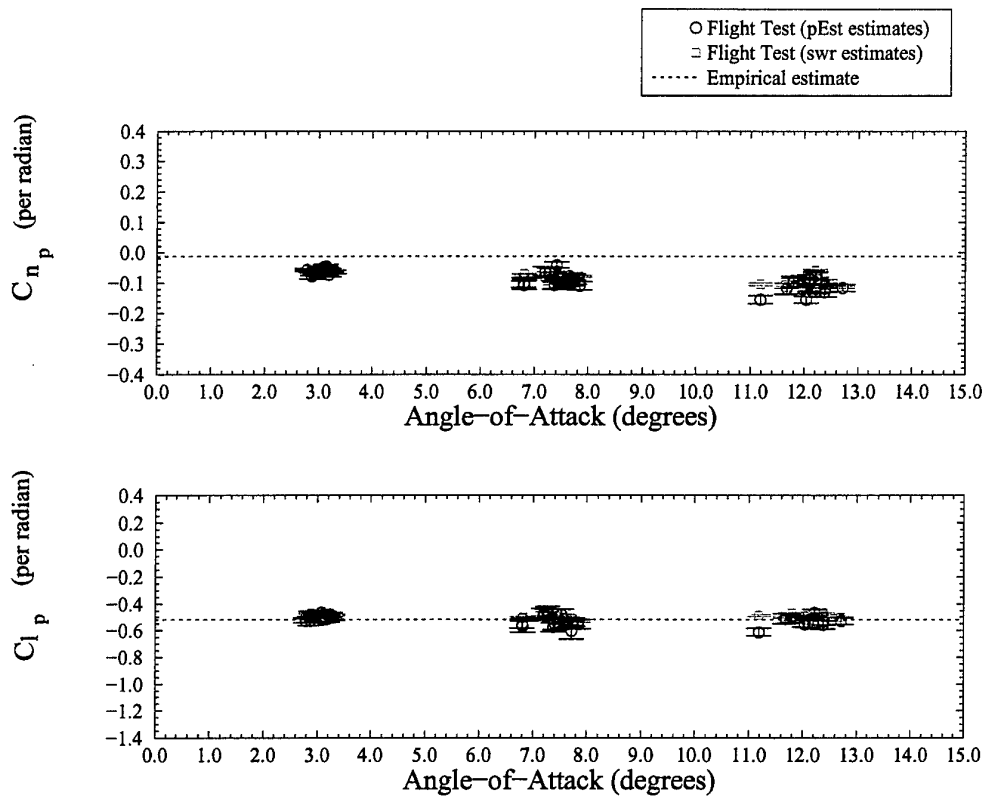


Figure 12: PC 9/A roll rate derivatives, 3-2-1 manoeuvres at 5000 ft.

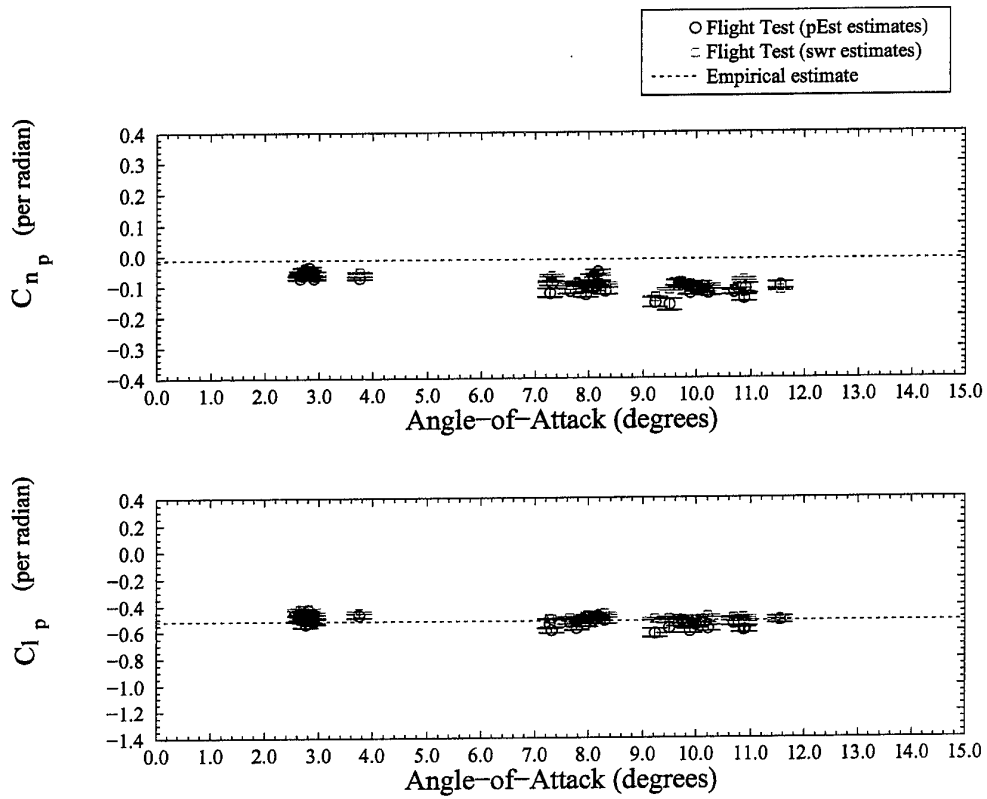


Figure 13: PC 9/A roll rate derivatives, 3-2-1-1 manoeuvres at 10 000 ft.

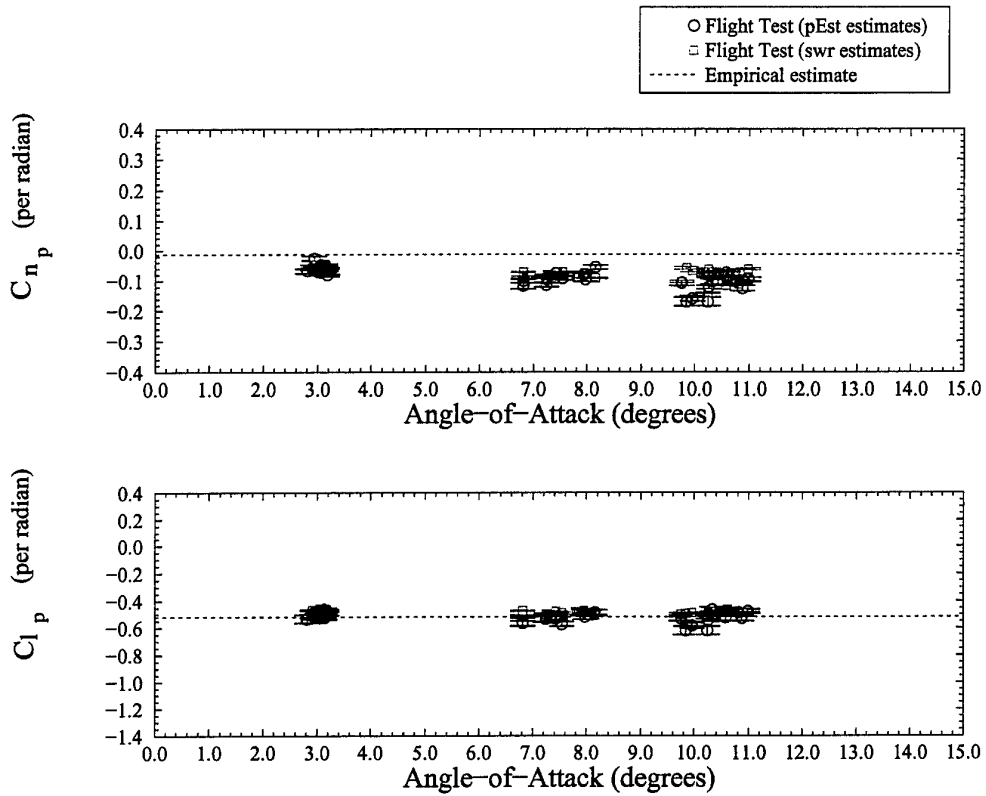


Figure 14: PC 9/A roll rate derivatives, 3-2-1 manoeuvres at 15 000 ft.

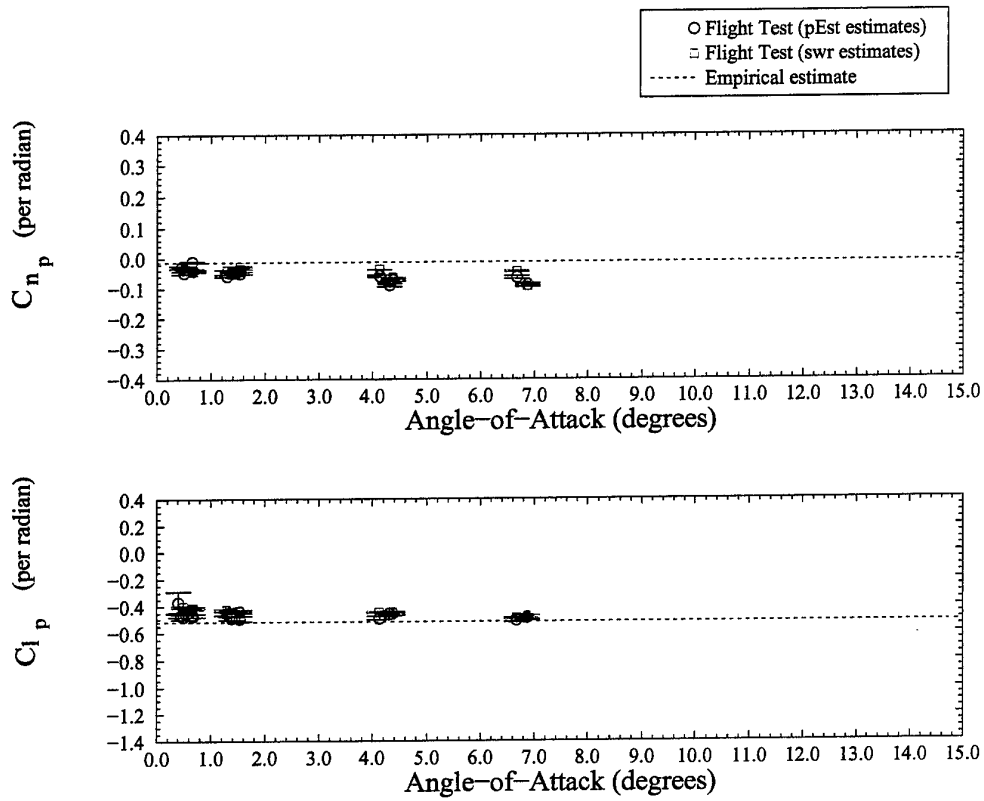


Figure 15: PC 9/A roll rate derivatives, doublet manoeuvres at 5000 ft.

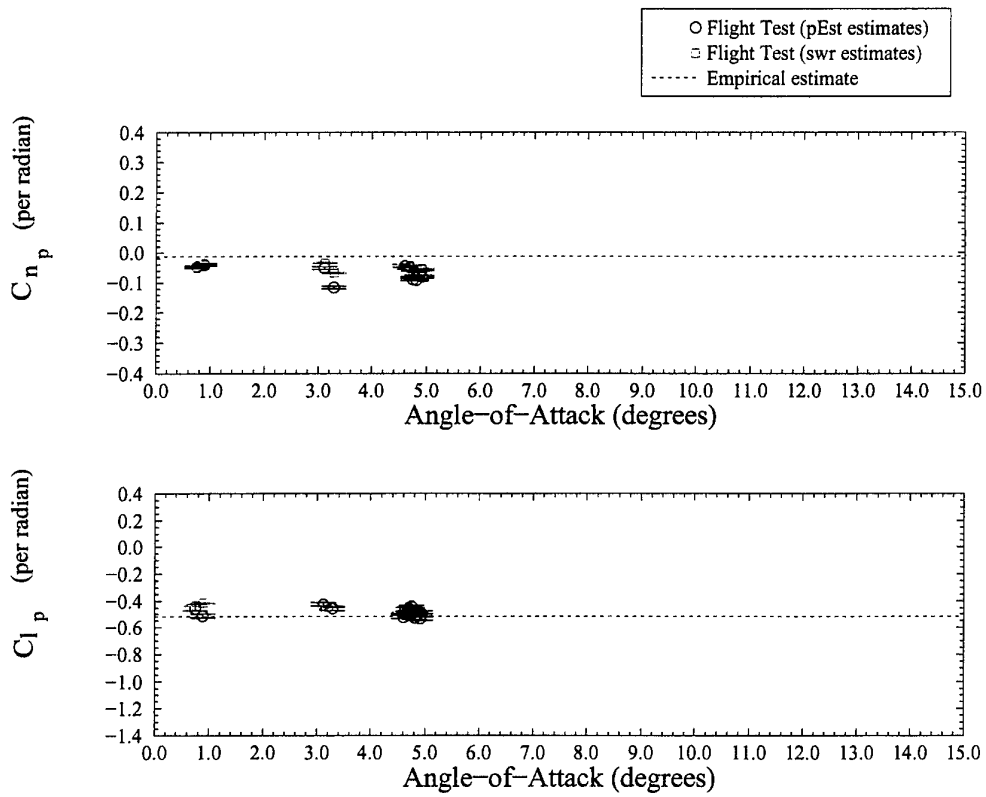


Figure 16: PC 9/A roll rate derivatives, doublet manoeuvres at 15 000 ft.

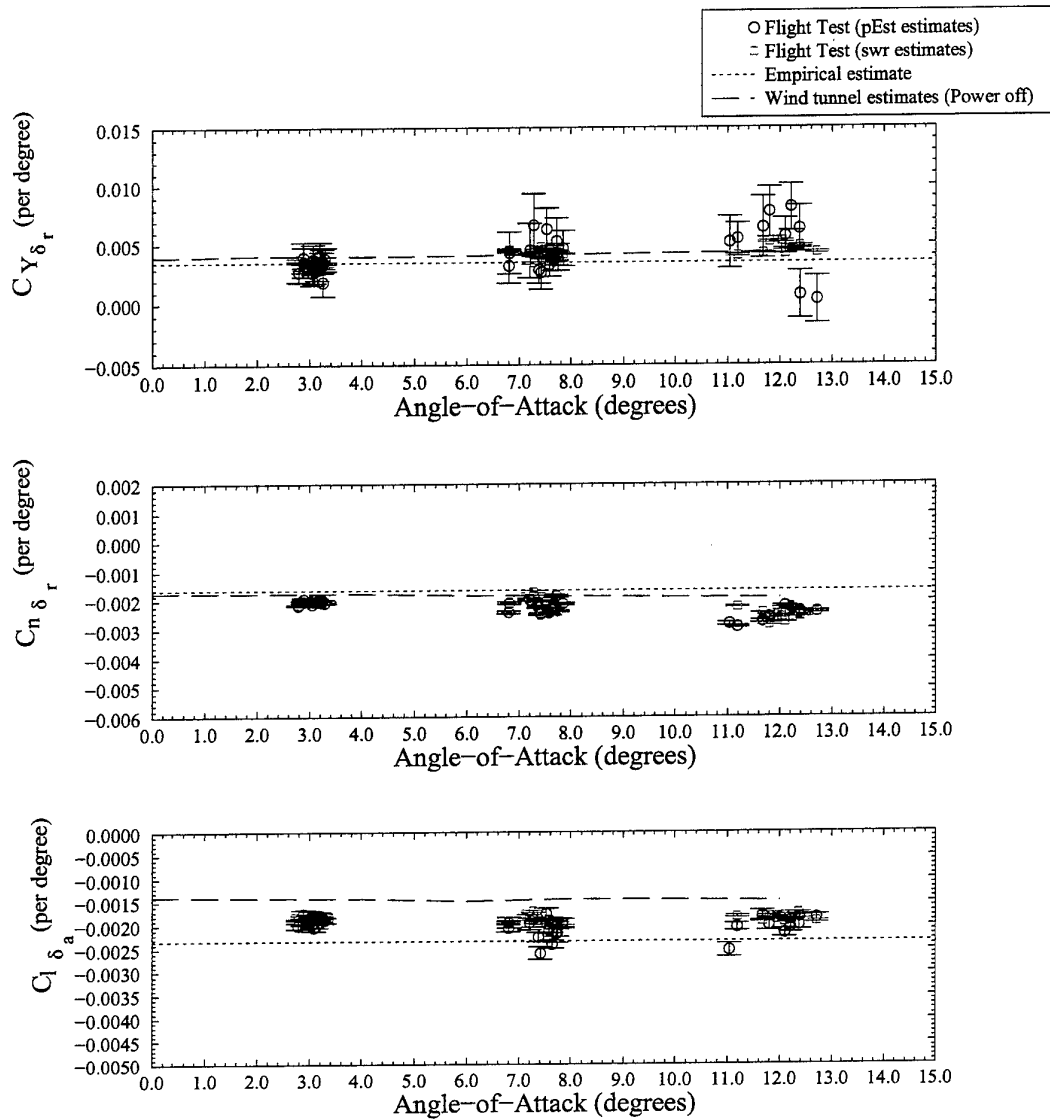
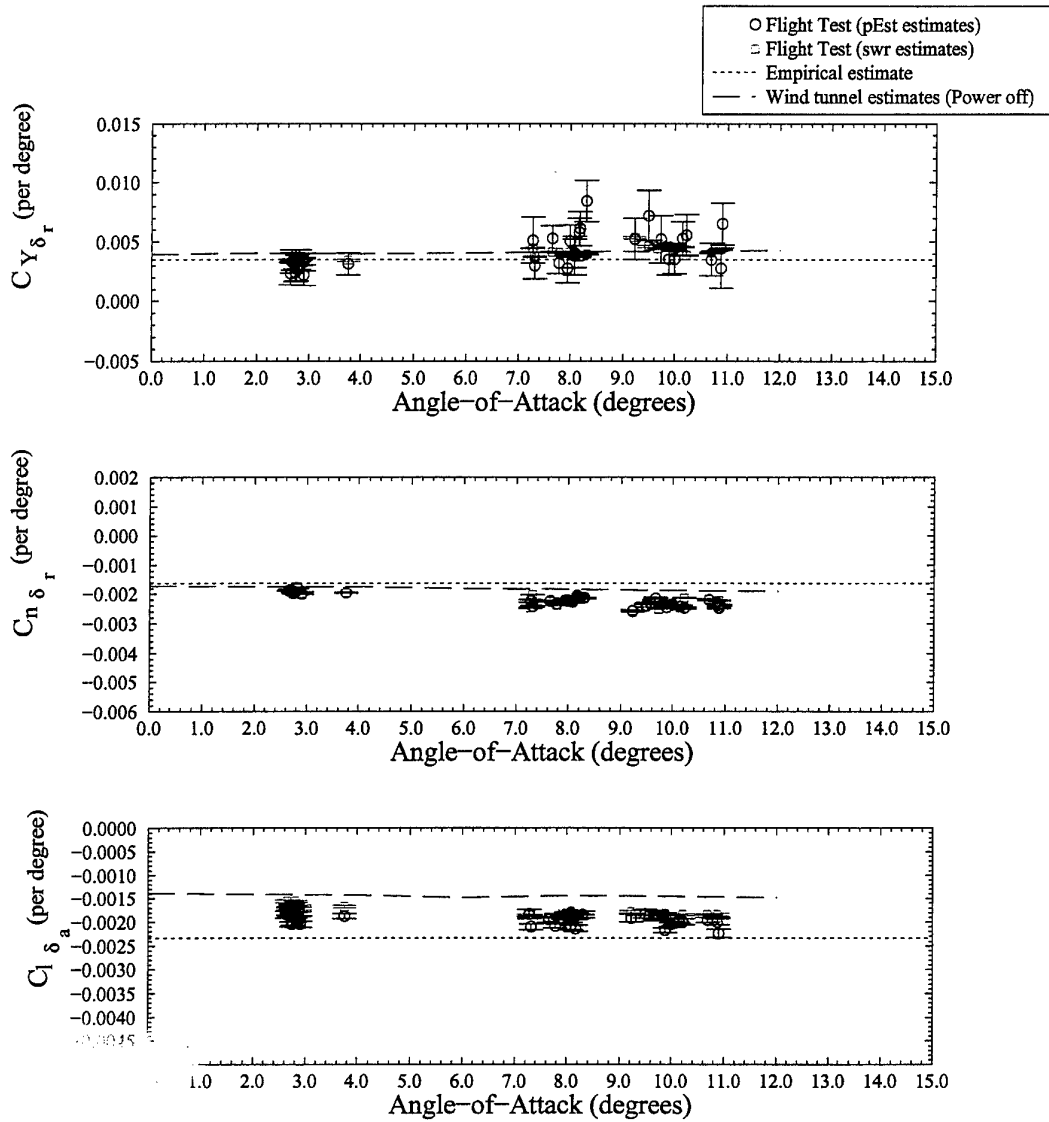


Figure 17: PC 9/A control derivatives, 3-2-1-1 manoeuvres at 5000 ft.



control derivatives, 3-2-1 manoeuvres at 10 000 ft.

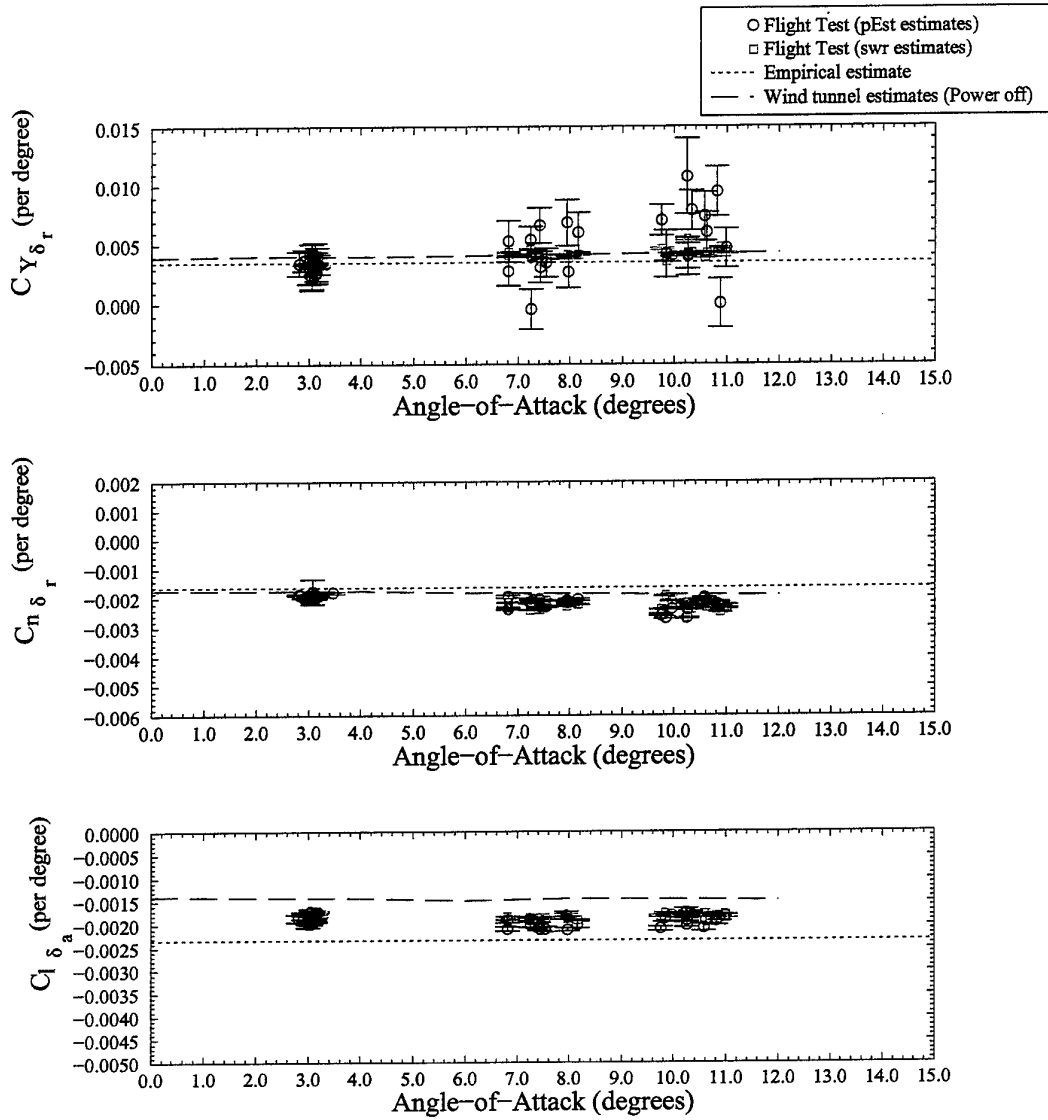


Figure 19: PC 9/A control derivatives, 3-2-1 manoeuvres at 15 000 ft.

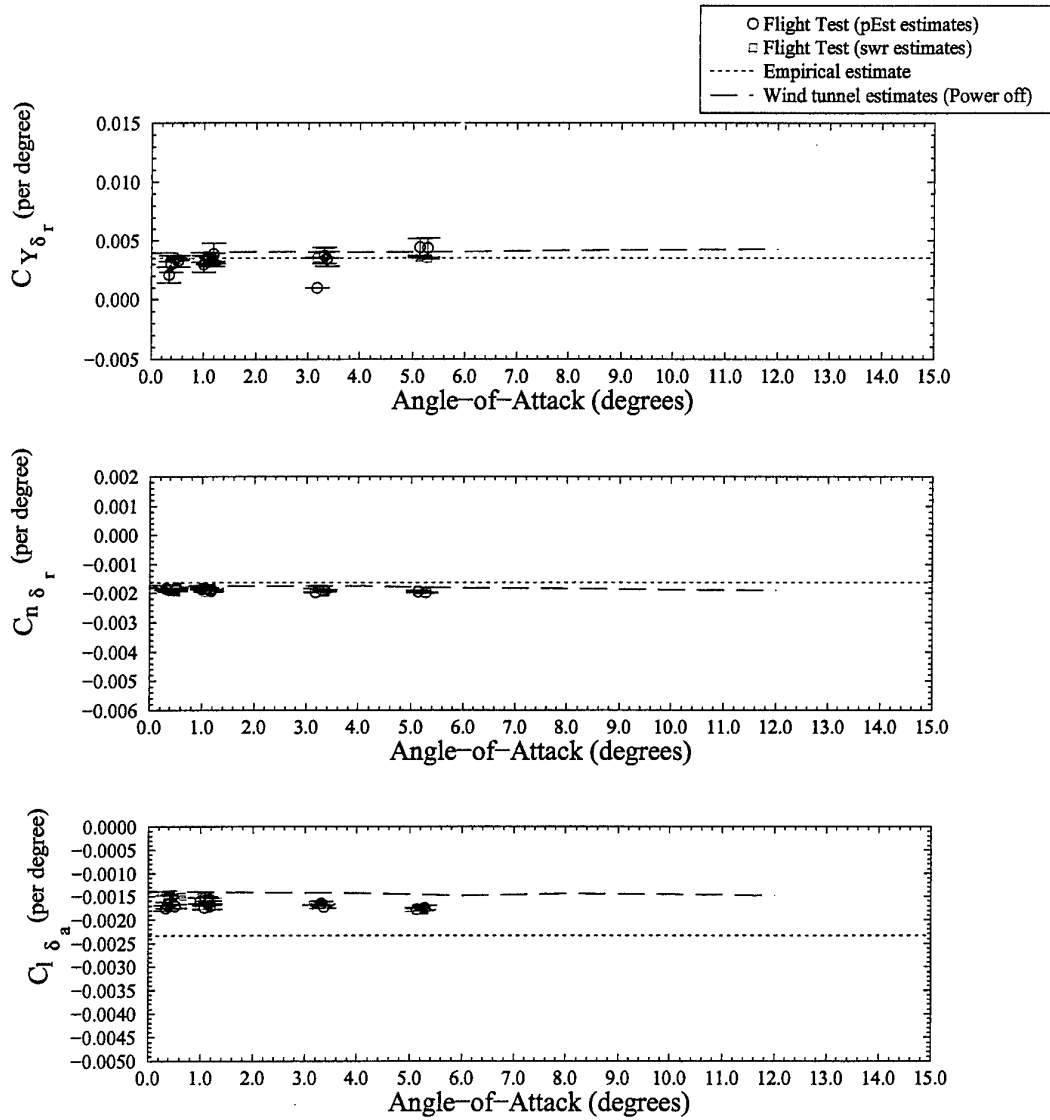


Figure 20: $C_{Y\delta_r}$, $C_{n\delta_r}$, $C_{l\delta_a}$ derivatives, doublet manoeuvres at 5000 ft.

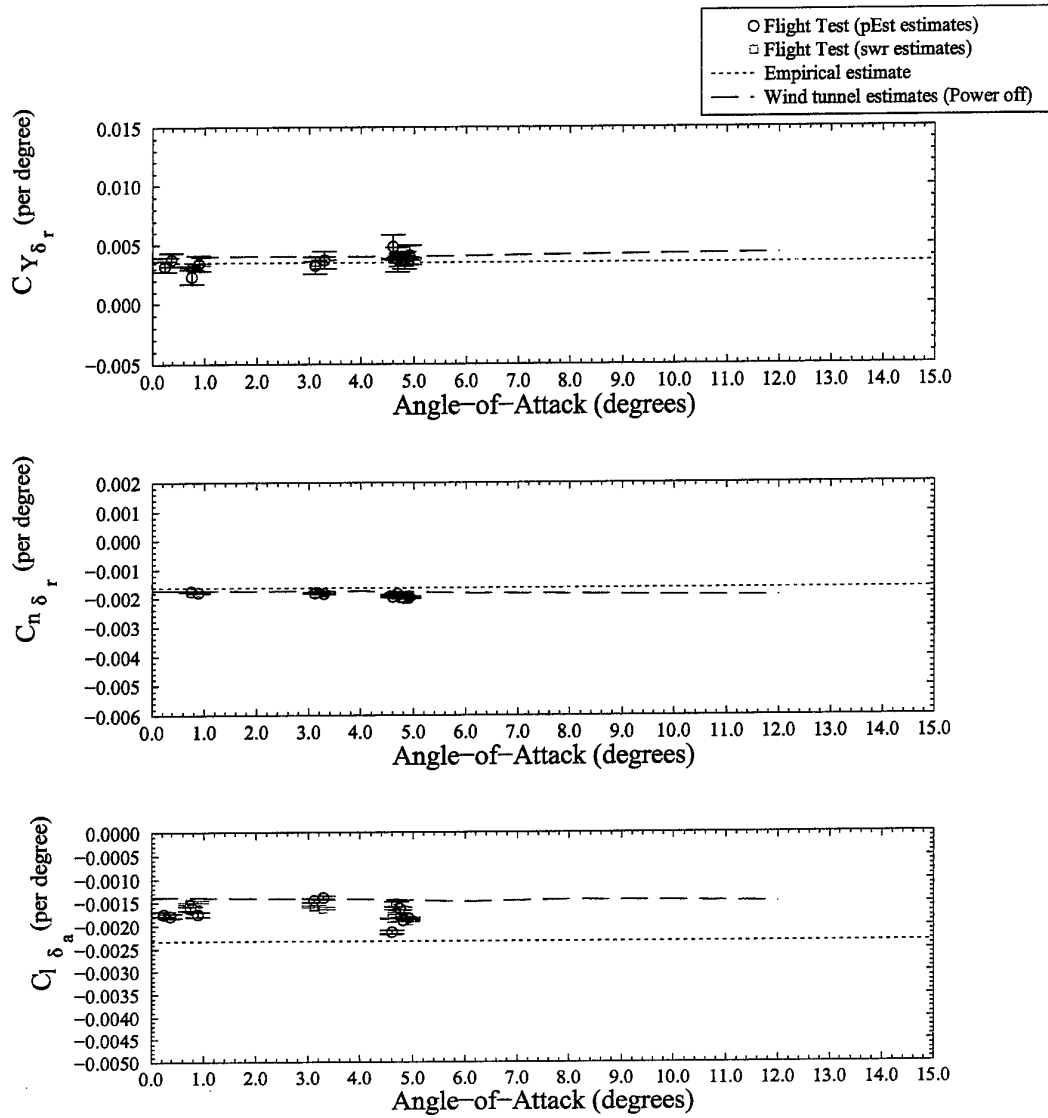


Figure 21: PC 9/A control derivatives, doublet manoeuvres at 15 000 ft.

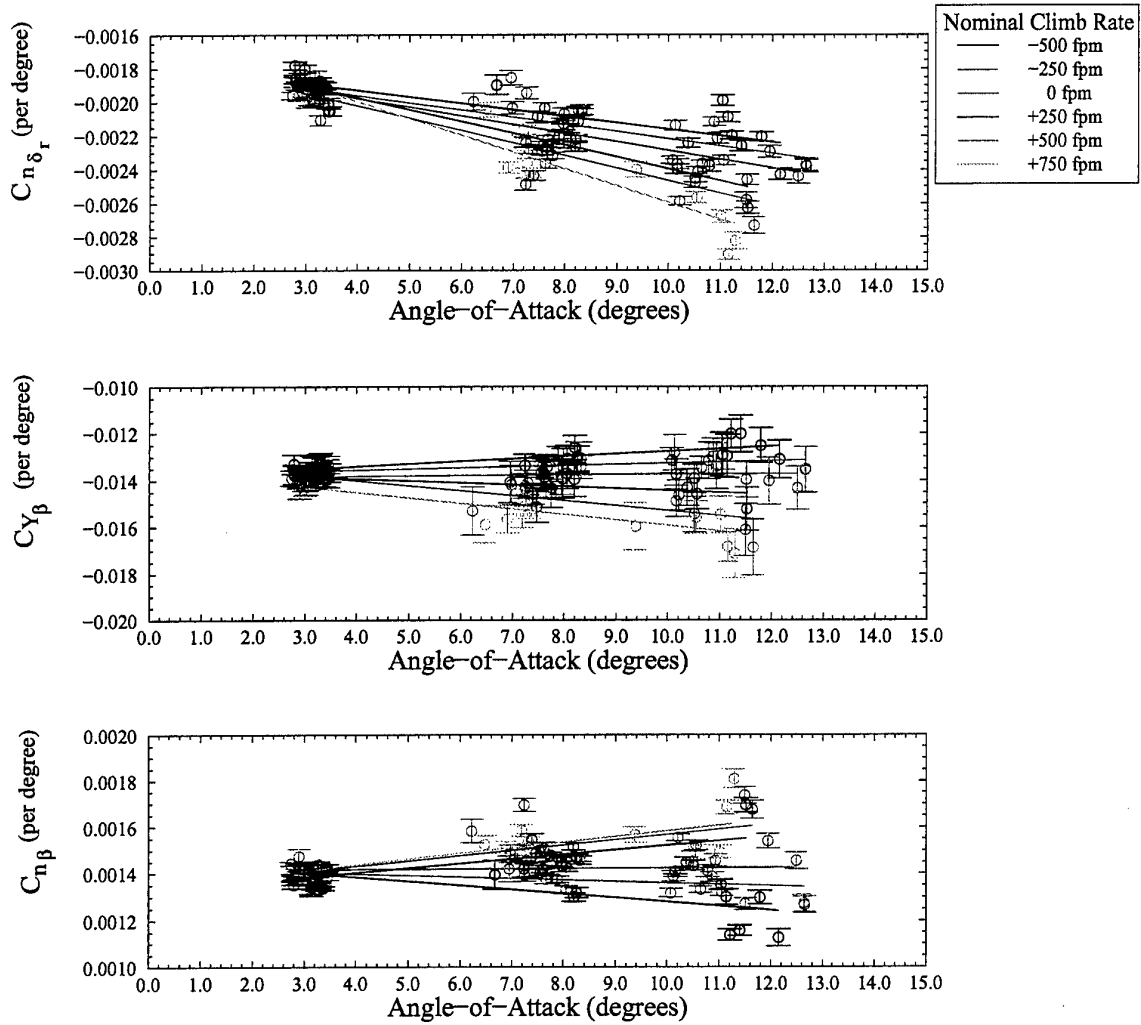


Figure 22: Variation of lateral derivatives with nominal rate of climb.

Appendix A: Weight, Centre-of-Gravity and Mass Moments-of-Inertia

The aircraft mass, centre-of-gravity and mass moments-of-inertia were determined for each test manoeuvre based on the aircraft fuel mass. The basic aircraft, pilot and fuel masses and moment arms from references [3] and [4] are given in table A1. The moment arms are measured relative to the aircraft datum, located 3m forward of the engine firewall, and 2m below the forward fuselage reference plane.

	Mass (kg)	Moment Arm (m)
Basic Aircraft	1784.5	4.306
Pilot	81.6	4.061
Fuel	Variable	4.178

Table A1: Flight test aircraft mass distribution [3, 4].

The mass of the aircraft is calculated as the sum of the basic aircraft, pilot and remaining fuel masses, by the following equation.

$$M = 1866.1 + M_F \quad (\text{kg}) \quad (\text{A1})$$

The longitudinal centre-of-gravity position of the flight test aircraft was determined from the following equation.

$$x_{c.g.} = \frac{8015.5 + 4.178M_F}{1866.1 + M_F} \quad (\text{m}) \quad (\text{A2})$$

During the flight test program, the aircraft longitudinal centre-of-gravity position varied between 4.27 m (24.2%MAC) and 4.30 m (25.6%MAC). The lateral and vertical centre-of-gravity positions were assumed to be invariant with fuel usage, and were fixed at values of 0.024 m and -2.2 m, respectively, relative to the aircraft datum.

The mass moments-of-inertia of the aircraft are given by the following equations.

$$I_{XX} = 2505.9 + 6.177(M - 1866.1) \quad (\text{kg.m}^2) \quad (\text{A3})$$

$$I_{YY} = 6622.2 + 0.033(M - 1866.1) \quad (\text{kg.m}^2) \quad (\text{A4})$$

$$I_{ZZ} = 8467.1 + 6.188(M - 1866.1) \quad (\text{kg.m}^2) \quad (\text{A5})$$

$$I_{XY} = 49.0 + 0.0057(M - 1866.1) \text{ (kg.m}^2\text{)} \quad (\text{A6})$$

$$I_{XZ} = 196.9 + 0.0041(M - 1866.1) \text{ (kg.m}^2\text{)} \quad (\text{A7})$$

$$I_{YZ} = 3.0 + 0.0007(M - 1866.1) \text{ (kg.m}^2\text{)} \quad (\text{A8})$$

Appendix B: Side Force, Rolling Moment and Yawing Moment Coefficients

An analysis was carried out on the PC 9/A flight test data to determine the relative contribution of each lateral derivative to the aircraft's force and moment coefficients, C_Y , C_n and C_l . This analysis was undertaken to confirm that contributions from derivatives set to their *a priori* values in the maximum likelihood analysis were not significant in the total force and moment equations of the aircraft. This analysis also confirmed the stepwise regression results, which showed several derivatives to be insignificant to the regression equation.

B.1 Side Force Coefficient

The side force coefficient may be represented by:

$$C_Y = C_{Y_0} + C_{Y_\beta} \beta + C_{Y_p} \left(\frac{pb}{2V} \right) + C_{Y_r} \left(\frac{rb}{2V} \right) + C_{Y_{\delta_a}} \delta_a + C_{Y_{\delta_r}} \delta_r \quad (\text{B1})$$

A comparison of the relative size of each component of the above equation is shown in figure B1 for a 3-2-1-1 manoeuvre. The results show that changes in side force are mainly due to the change in the aircraft's angle-of-sideslip. The roll rate and rudder deflection contributions to side force are small, while yaw rate and aileron deflection contributions are negligible.

B.2 Yawing Moment Coefficient

The yawing moment coefficient may be represented by:

$$C_n = C_{n_0} + C_{n_\beta} \beta + C_{n_p} \left(\frac{pb}{2V} \right) + C_{n_r} \left(\frac{rb}{2V} \right) + C_{n_{\delta_a}} \delta_a + C_{n_{\delta_r}} \delta_r \quad (\text{B2})$$

A comparison of the relative size of each component of the above equation is shown in figure B2 for a 3-2-1-1 manoeuvre. The results show that the yaw stiffness derivative, C_{n_β} , and the yaw control derivative, $C_{n_{\delta_r}}$, are important, while the remaining derivatives are less significant to the total yawing moment coefficient of the aircraft.

B.3 Rolling Moment Coefficient

The rolling moment coefficient may be represented by:

$$C_l = C_{l_0} + C_{l_\beta} \beta + C_{l_p} \left(\frac{pb}{2V} \right) + C_{l_r} \left(\frac{rb}{2V} \right) + C_{l_{\delta_a}} \delta_a + C_{l_{\delta_r}} \delta_r \quad (\text{B3})$$

A comparison of the relative size of each component of the above equation is shown in Figure B1 for a -2-1-1 manoeuvre. With the exception of $C_{l_{\delta_r}}$, each of the rolling moment components is significant to the total rolling moment coefficient of the aircraft.

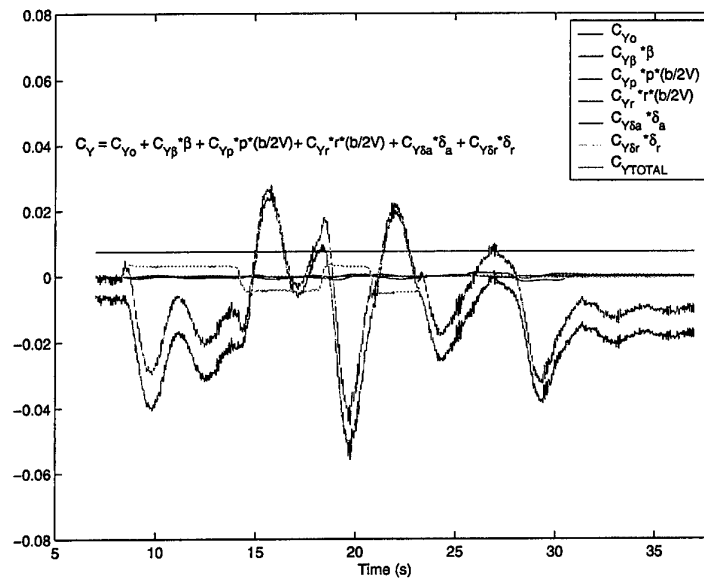


Figure B1: Relative magnitudes of C_Y equation components.

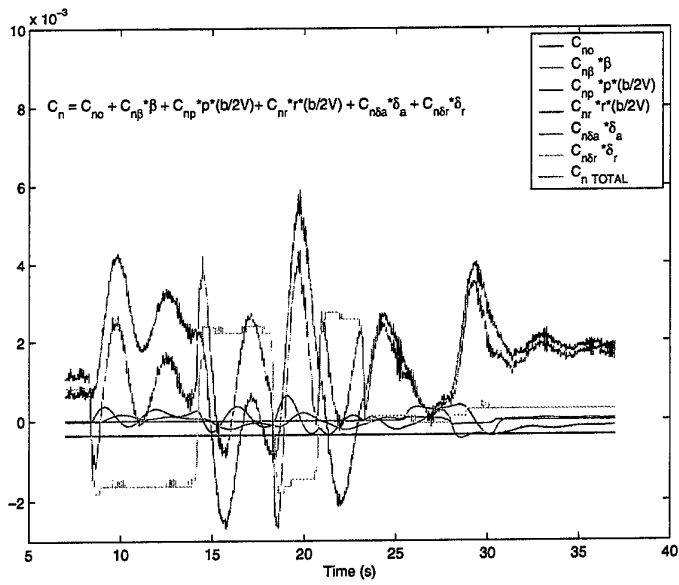


Figure B2: Relative magnitudes of C_n equation components.

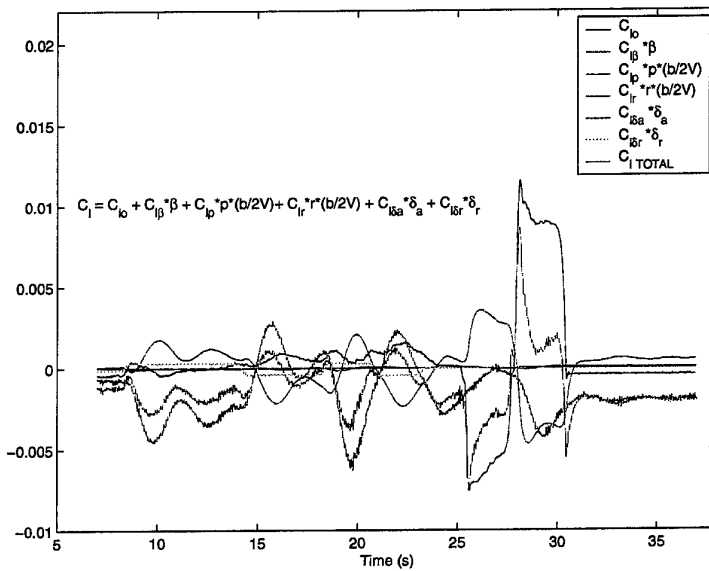


Figure B3: Relative magnitudes of C_1 equation components.

DISTRIBUTION LIST

A Correlation between Flight-determined Lateral Derivatives and Ground-based Data for
the Pilatus PC 9/A Training Aircraft in Cruise Configuration

Hilary A. Keating, Nick van Bronswijk, Andrew D. Snowden and Jan S. Drobik

Number of Copies

DEFENCE ORGANISATION

Task Sponsor

COPS HQAC 1

S&T Program

Chief Defence Scientist	}	
FAS Science Policy		1
AS Science Corporate Management		

Director General Science Policy Development 1

Counsellor, Defence Science, London Doc Data Sht

Counsellor, Defence Science, Washington Doc Data Sht

Scientific Adviser to MRDC Thailand Doc Data Sht

Scientific Adviser Policy and Command 1

Navy Scientific Adviser Doc Data Sht

Scientific Adviser, Army Doc Data Sht

Air Force Scientific Adviser 1

Director Trials 1

Aeronautical and Maritime Research Laboratory

Director, Aeronautical and Maritime Research Laboratory 1

Air Operations Division

Chief, Air Operations Division 1

Research Leader, Avionics and Flight Mechanics 1

Head, Flight Mechanics Applications 1

Task Manager - G. J. Brian 1

Author - H. A. Keating 1

Author - N. van Bronswijk 1

Author - A. D. Snowden 1

Author - J. S. Drobik 1

B. A. Woodyatt 1

K. L. Bramley 1

DSTO Research Library and Archives

Library Fishermans Bend 1

Library Maribyrnong	1
Library Salisbury	2
Library, MOD, Pyrmont	Doc Data Sht
US Defense Technical Information Center	2
UK Defence Research Information Centre	2
Canada Defence Scientific Information Service	1
NZ Defence Information Centre	1
National Library of Australia	1
Capability Systems Staff	
Director General Maritime Development	Doc Data Sht
Director General C3I Development	Doc Data Sht
Director General Aerospace Development	1
Aircraft Research and Development Unit	
MSSUP1	1
Intelligence Program	
DGSTA Defence Intelligence Organisation	1
Manager, Information Centre, Defence Intelligence Organisation	1
Corporate Support Program	
Officer in Charge, TRS, Defence Regional Library, Canberra	1
UNIVERSITIES AND COLLEGES	
Australian Defence Force Academy Library	1
Head of Aerospace and Mechanical Engineering, ADFA	1
Deakin University Library, Serials Section (M List)	1
Librarian, Flinders University	1
Head of Aeronautical Engineering, University of Sydney	1
Head of Centre of Expertise in Aerodynamic Loading, RMIT	1
Adrian Pearce, Computer Science, Curtin University WA	1
OTHER ORGANISATIONS	
NASA (Canberra)	1
Info Australia	1
ABSTRACTING AND INFORMATION ORGANISATIONS	
Library, Chemical Abstracts Reference Service	1
Engineering Societies Library, US	1

Materials Information, Cambridge Science Abstracts, US	1
Documents Librarian, The Center for Research Libraries, US	1

INFORMATION EXCHANGE AGREEMENT PARTNERS

Acquisitions Unit, Science Reference and Information Service, UK	1
Library - Exchange Desk, National Institute of Standards and Technology, US	1
National Aerospace Library, Japan	1
National Aerospace Library, Netherlands	1

SPARES

H. A. Keating	5
---------------	---

Total number of copies:	55
--------------------------------	-----------

DEFENCE SCIENCE AND TECHNOLOGY ORGANISATION DOCUMENT CONTROL DATA				1. CAVEAT/PRIVACY MARKING	
2. TITLE A Correlation between Flight-determined Lateral Derivatives and Ground-based Data for the Pilatus PC 9/A Training Aircraft in Cruise Configuration			3. SECURITY CLASSIFICATION Document (U) Title (U) Abstract (U)		
4. AUTHORS Hilary A. Keating, Nick van Bronswijk, Andrew D. Snowden and Jan S. Drobik			5. CORPORATE AUTHOR Aeronautical and Maritime Research Laboratory 506 Lorimer St, Fishermans Bend, Victoria, Australia 3207		
6a. DSTO NUMBER DSTO-TR-0988		6b. AR NUMBER AR-011-475	6c. TYPE OF REPORT Technical Report		7. DOCUMENT DATE June, 2000
8. FILE NUMBER M1/9/746	9. TASK NUMBER AIR 97/135	10. SPONSOR COPS HQAC	11. No OF PAGES 38	12. No OF REFS 20	
13. URL OF ELECTRONIC VERSION http://www.dsto.defence.gov.au/corporate/reports/DSTO-TR-0988.pdf			14. RELEASE AUTHORITY Chief, Air Operations Division		
15. SECONDARY RELEASE STATEMENT OF THIS DOCUMENT <i>Approved For Public Release</i> <small>OVERSEAS ENQUIRIES OUTSIDE STATED LIMITATIONS SHOULD BE REFERRED THROUGH DOCUMENT EXCHANGE, PO BOX 1500, SALISBURY, SOUTH AUSTRALIA 5108</small>					
16. DELIBERATE ANNOUNCEMENT No Limitations					
17. CITATION IN OTHER DOCUMENTS No Limitations					
18. DEFTEST DESCRIPTORS Aerodynamics Aerodynamic stability Lateral stability System identification Aerodynamic configurations Flight tests PC 9/A aircraft					
19. ABSTRACT A series of flight tests were conducted on the PC 9/A aircraft, A23-045, at the Royal Australian Air Force's Aircraft Research and Development Unit. System identification techniques were applied to the data obtained from these flight tests to determine the stability and control derivatives of the aircraft. The lateral results for the aircraft in cruise configuration are presented in this report and comparisons are made with empirical and ground based estimates.					